Short title:

Selaginella Root Bifurcation

Corresponding author:

Tom Beeckman

VIB Center for Plant Systems Biology

Ghent University, Department of Plant Biotechnology

Technologiepark 71

B-9052 Ghent (Belgium)

Tel.: +32 9 3313830; Fax: +32 9 3313809; E-mail: tom.beeckman@psb.vib-ugent.be

Cellular and gene expression patterns associated with root bifurcation in *Selaginella*

Tao Fang,[a,b,2] Hans Motte,[a,b,2] Boris Parizot,[a,b] Wouter Smet,[a,b] Xilan Yang,[a,b] Liam Walker,[c] Maria Njo,[a,b] George W. Bassel,[c] and Tom Beeckman,[a,b,3,4]

[a]Department of Plant Biotechnology and Bioinformatics, Ghent University, 9052 Ghent, Belgium

[b]VIB Center for Plant Systems Biology, 9052 Ghent, Belgium

[c]School of Life Sciences, University of Warwick, Coventry, CV4 7AL, UK

ORCID IDs: 0000-0002-9903-6956 (T.F.); 0000-0002-6059-1397 (H.M.); 0000-0003-1445-6925 (B.P.); 0000-0002-8000-3097 (W.S); 0000-0001-9499-9991 (X.Y.); 0000-0003-0261-0518 (L.W.); 0000-0001-7285-5954 (M.N.); 0000-0002-3434-4499 (G.W.B.); 0000-0001-8656-2060 (T.B.)

One-sentence summary:

The root of the spike moss *Selaginella moellendorffii* bifurcates following a symmetric cell division of the single stem cell and involves conserved genetic modules known from angiosperm roots.

Footnotes:

[1] This study was financially supported by the Fonds voor Wetenschappelijk Onderzoek – Vlaanderen (FWO)-project G027313N and G028421N. T.F. was financially supported by China Scholarship Council and the Erasmus Mundus programme of the European Union (Lotus Unlimited Project). L.W. and G.W.B. were supported by BBSRC grant BB/S002804/1.
[2]These authors contributed equally to the article.
[3]Author for contact: tom.beeckman@psb.vib-ugent.be.
[4]Senior author.

The author responsible for distribution of materials integral to the findings presented in this article in accordance with the policy described in the Instructions for Authors (www.plantphysiol.org) is: Tom Beeckman (tom.beeckman@psb.vib-ugent.be).

T.F., H.M., B.P. and T.B. designed the experiments. T.F., X.Y., W.S. and M.N. collected microscopic data. T.F., W.S., L.W. and G.W.B. processed microscopic data. T.F., H.M. and B.P. performed the RNA-seq experiment. B.P. processed the transcriptomic dataset. H.M. and B.P. analyzed the transcriptomic dataset. H.M. and T.B. supervised the project. T.F., H.M. and T.B. wrote the manuscript. All the authors read and approved the final manuscript.

Abstract

The roots of lycophytes branch through dichotomy or bifurcation, which means that the root apex splits into two daughter roots. This is morphologically distinct from lateral root (LR) branching in the extant euphyllophytes, where LRs develop along the root axis at different distances from the apex. The process of root bifurcation is poorly understood, while such knowledge can be important, as it may represent an evolutionarily ancient strategy that roots recruited to form new stem cells or meristems. In this study, we examined root bifurcation in the lycophyte *Selaginella moellendorffii*. We characterized an *in vitro* developmental time-frame based on repetitive apex bifurcations, allowing us to sample different stages of dichotomous root branching and analyze the root meristem and root branching in *S. moellendorffii* at the microscopical and transcriptional level. Our results show that, in contrast to previous assumptions, initial cells in the root meristem are mostly not tetrahedral but rather show an irregular shape. Tracking down the early stages during root branching argues for the occurrence of a symmetric division of the single initial cell resulting in two apical stem cells allowing for root meristem bifurcation. Moreover, we generated a *S. moellendorffii* root branching transcriptome, which resulted in the delineation of a subset of core meristem genes. The occurrence of multiple meristem-related orthologues in this dataset, including inversely correlated expression profiles of a *SCARECROW* (*SCR*) versus a *RETINOBLASTOMA-RELATED1* (*RBR1*) homologue suggests the presence of conserved pathways in the control of meristem and root stem cell establishment or maintenance.

Key words: *Selaginella moellendorffii*, meristem bifurcation, initial cell, evolution, root apical meristem.

72 Roots provide multiple key functions for plants, and their capacity to branch is
73 important to anchor in a substrate and to forage for water and nutrients (Raven and
74 Edwards, 2001; Motte et al., 2019). Root development and root branching have been in
75 particular studied in angiosperms, e.g. Arabidopsis. Here, roots branch via the
76 formation of lateral roots (LRs), which develop in the differentiated part of the root
77 from pluripotent pericycle cells. After a series of well-orchestrated divisions, a new root
78 meristem is formed that grows out of the parent root. Interestingly, important insights
79 into the anatomical development and molecular regulation of LR formation were
80 obtained by employing LR inducible systems, allowing synchronous induction of many
81 LRs (Himanen et al., 2002; Himanen et al., 2004; Vanneste et al., 2005; De Smet et al.,
82 2008; De Rybel et al., 2010; Jansen et al., 2013; Xuan et al., 2015; Crombez et al., 2016;
83 Herrbach et al., 2017).
84 In contrast to angiosperms, Selaginella species, members of the lycophyte lineage,
85 do not possess pluripotent cells that give rise to LRs (Fang et al., 2019). Instead, roots
86 dichotomously branch at the tip through bifurcation of the apical meristem (Imaichi and
87 Kato, 1989; Lu and Jernstedt, 1996; Otręba and Gola, 2011; Gola, 2014; Fang et al.,
88 2019; Motte and Beeckman, 2019). Lycophytes were the first plants that developed
89 roots (Hetherington and Dolan, 2018). Hence, studying their root system can contribute
90 to the understanding of how root developmental mechanisms evolved. Lycophyte roots,
91 however, originated independently from roots in the other land plant lineages
92 (Hetherington and Dolan, 2019), but both molecular and anatomical data suggest a
93 highly convergent evolution, and possibly even a common (partial) recruitment of a
94 genetic program present in the rootless common ancestor of the different lineages
95 (Huang and Schiefelbein, 2015; Motte and Beeckman, 2019). Based on fossil records,
96 dichotomous root branching was found at the base of lycophyte evolution, putting it
97 forward as an early innovation during the evolution of roots (Hao et al., 2010;
98 Matsunaga and Tomescu, 2016; Hetherington and Dolan, 2017; Hetherington et al.,
99 2020).

100 Unfortunately, despite intensive, but almost exclusively histological studies, the
101 development and anatomy of the Selaginella root apical meristem and its bifurcation
102 are still poorly understood. Multiple studies report the presence of one central
103 tetrahedral initial cell (IC) or apical stem cell (Otręba and Gola, 2011 and refs therein)
104 that, in analogy with the apical cell in the root meristem of certain ferns, was suggested
105 to cut off daughter cells in four directions to provide cells for the root cap at the distal
106 side, and cells for the growing root at the three proximal sides. In some ferns, it is
107 clearly documented that the three proximal daughter cells each divide in an equal
108 pattern, forming merophytes or clonally related groups of cells. Subsequent merophytes
109 are superimposed to form different layers in the root (Hou and Hill, 2004). In contrast
110 to ferns, such division pattern is less obvious in Selaginella roots. Furthermore, the
111 branching process is problematic to study at the microscopical level. Live imaging is
112 difficult due to the lack of biotechnological tools (Motte et al., 2020) and arbitrarily
113 sampled roots rarely represent critical phases in which roots are undergoing bifurcation.
114 Moreover, histological sectioning does not allow a high-throughput approach, and serial
115 sectioning is required to obtain the relevant sections in which the IC is visible. As a
116 consequence, the cell division events associated with root meristem bifurcation remain
117 elusive, and different hypotheses still exist on how the doubling of the meristem might
118 occur (Motte and Beeckman, 2019). One hypothesis suggests the disappearance of the
119 IC due to segmentation followed by the recruitment of two new meristematic cells as
120 two new ICs (Otręba and Gola, 2011). Barlow and Lück (2004), on the other hand,
121 suggested that one of the daughter cells of the original IC becomes a new initial.
122 Interestingly, in the Selaginella shoot meristem, a seemingly symmetric division of the
123 apical cell initiates dichotomy (Jones and Drinnan, 2009). Such a symmetric
124 longitudinal division of the apical cell is also the cause of thallus bifurcation in certain
125 algae (Oltmanns, 1889; von Goebel, 1928; van den Hoek et al., 1995; Gola, 2014).
126 Being the first lycophyte with a sequenced genome, *S. moellendorffii* became an
127 important model species for evolutionary research (Banks, 2009; Banks et al., 2011;

128 Motte et al., 2020). Moreover, as root bifurcation seems to involve the initiation of a
129 new root stem cell, dichotomous root branching could be used as a unique system to
130 study root stem cell specification in an evolutionary context and to get insight into the
131 complex process of dichotomy in general. Useful datasets and genetic tools start to
132 become available, including several transcriptomic datasets from root samples (Ferrari
133 et al., 2020; Motte et al., 2020; Fang et al., 2021). However, these studies are merely
134 snapshots of the roots and do not allow to study temporal changes associated with the
135 bifurcation process.

136 *S. moellendorffii* root branching cannot be induced by hormone treatments and a
137 root branching inducible system, similar as for angiosperms, does not seem to be
138 feasible (Fang et al., 2019), complicating the capturing of early bifurcating root
139 meristems. Here, as an alternative, we developed a dichotomous branching time course
140 assay to enrich for samples with bifurcating roots. We applied this assay for histological
141 sectioning and whole-mount confocal microscopy. Based on this, and complementary
142 to the current literature, we advocate that two new root meristems originate due to a
143 symmetric division of the IC into two ICs. Furthermore, we exploited the assay to
144 sample roots at regular intervals for RNA sequencing (RNA-seq) and revealed as such
145 the *S. moellendorffii* root branching transcriptome. We show that transiently
146 upregulated genes have a meristem signature, supporting the value of this dataset as a
147 useful resource to identify candidate stem cell or meristem regulators in Selaginella.
148 Moreover, a vast number of differentially expressed genes are homologous to
149 Arabidopsis genes with a known role in stem cell or meristem functioning. This
150 indicates, despite the structural difference in root meristems between Selaginella and
151 Arabidopsis, a strong conservation in the pathways controlling meristem or stem cell
152 functionality.
153

154 # RESULTS

155 ## Developmental Time Frames of *S. moellendorffii* Root Bifurcation

156 The study of root bifurcation or branching in *S. moellendorffii* would take
157 advantage of an inducible root branching system like the LR inducible system in
158 Arabidopsis (Himanen et al., 2002). The added value of using such a system is that the
159 initiation of new meristems can be synchronized and thus followed over time. A
160 prerequisite is, however, to obtain a zero point at which no branching is ongoing. We
161 previously reported that auxin transport inhibitors and a synthetic cytokinin were not
162 useful to prevent root branching in *S. moellendorffii*, without affecting growth, and as
163 such do not allow to obtain uniform starting material. Moreover, we did not succeed to
164 identify a treatment that could induce meristem bifurcation itself (Fang et al., 2019). As
165 a consequence, a synchronized root branching system that enables the study of root
166 branching initiation does not seem to be feasible.

167 Therefore, we asked whether we could predict root branching based on the
168 repetitive apex divisions taking place in *in vitro*-grown *S. moellendorffii* explants as an
169 alternative approach. To characterize root branching, *S. moellendorffii* shoot explants
170 were excised and transferred on fresh medium, which resulted in the spontaneous
171 development of roots. First rhizophores were initiated, from which the root grew out
172 (Fig. 1, A and B); subsequently, the roots repeatedly bifurcated dichotomously
173 (Fig. 1, C and D; Supplemental Movie S1) (see also Fang et al., 2019). We followed the
174 origin and bifurcation of in total 983 roots within three independent experiments, and
175 observed all roots on a daily basis. Bifurcation events were macroscopically observed
176 and recognized by the presence of two dome-shaped primordia at the root tip (Fig. 1C).
177 In practice, it was difficult to exactly trace back the time of appearance for all
178 rhizophores, as young rhizophores were almost colorless and mostly covered by the
179 leaves. Still, taking the time point of the shoot explant transfer as the reference, we
180 observed that a majority of the roots underwent the first bifurcation in a relatively short
181 time span, more particularly, between 10 and 15 d post transfer of the explants (Fig. 1E).

182 We continued to follow a subset of 361 root tips from two experimental repeats, and
183 observed, taking the first bifurcation (Fig. 1C) as a reference point, a consistent short
184 time frame for the second root bifurcation, which occurred in the majority of roots
185 between 6 and 9 d after the first bifurcation (Fig. 1F). Hence, as the dichotomous
186 branching seemed to occur according to a relatively regular periodicity, the branching
187 time could be roughly predicted.

188 To study the timing of bifurcation in more detail at the histological level, we took
189 the first bifurcation event as shown in Figure 1C as reference time point 0, and sampled
190 at least ten root tips on a daily basis for microscopic analysis. All root tips were
191 subjected to whole-mount confocal imaging to assess the appearance new meristems,
192 as shown in Figure 1G. As previously shown, the apices at time point 0 never contained
193 two apical meristems (Fang et al., 2019). Similarly, meristem bifurcation was not
194 detected on the first and second day after the first branching (Fig. 1H). The first roots
195 with two clear meristem regions were detected 3 d after the first branching. The number
196 of roots with two meristem regions steadily increased over time and almost all root tips
197 effectively bifurcated after 6 d (Fig. 1H).

198 Thus, in a relatively limited time frame after the first bifurcation event, practically
199 all root tips bifurcated again. Because the presence of two meristems was visible from
200 day 3 onwards, the onset of the bifurcation and related anatomical events could be
201 anticipated to occur early during the time course. Furthermore, due to the steadily
202 increasing percentage of bifurcated meristems, we could anticipate the enrichment of
203 specific developmental stages during consecutive time points. Therefore, we employed
204 this time course starting from newly branched roots to further characterize *S.*
205 *moellendorffii* root branching, both from the histological and molecular point of view.

206 Meristem Bifurcation Is the Result of a Symmetric Division of an 207 Irregularly Shaped IC

208 To characterize the early events in *S. moellendorffii* root branching, we sampled

209 root tips on different days after the first bifurcation event (time point 0) and subjected
210 them to histological sectioning. At time point 0, two root tips are present each with an
211 IC in the center of the meristem (Fig. 2, A and B). Within the meristems, merophytic
212 cell clusters next to the IC with triangular shape could be easily recognized, illustrating
213 how daughter cells have been cut off from different faces of the IC, and subsequently
214 divided (Fig. 2B). Starting from two days after time point 0, we were able to recognize
215 two similar-sized ICs next to or close to each other in different root tips (Fig. 2, C-G).
216 This challenges the current hypotheses on the initiation of dichotomous root branching
217 in Selaginella, and might point to a rather symmetric division of this IC as a first stage
218 during root bifurcation. In particular Figure 2C shows a clear image of two separate
219 basal derivatives from the presumptive ICs that form root cap cells. Figure 2D shows a
220 similar image, but here, one of the two presumptive ICs has two nuclei and is finishing
221 a cell division. Figure 2E and F show root apices with two presumptive ICs separated
222 by only one cell, while Figure 2G shows a separation of the two ICs by more cells.
223 Overall, this indicates that two new ICs originate after a symmetric division, and
224 continue to develop two new root primordia.

225 However, in many samples, we were not able to recognize such stages, and
226 designation of the ICs was often not straightforward, possibly because ICs were
227 regularly out of plane in the sections. Therefore, to confirm the observed and seemingly
228 symmetric divisions of the IC, and to increase the workflow in order to analyze more
229 samples at the same time, we decided to use the same approach by performing whole-
230 mount confocal imaging. Supplemental Movie S2 shows a full stack of an unbranched
231 root, and illustrates how this technique enables better designation of the IC by going
232 through the sections. This stack was used to reconstruct the root (Fig. 3A) and clearly
233 present the organization of the meristem. To have a better view on the structure of the
234 IC, we first used whole stacks for 3D cell segmentation and isolated the IC. Earlier
235 reports with two-dimensional histological sections hypothesized that the root IC is
236 tetrahedral (Imaichi and Kato, 1989; Otręba and Gola, 2011). However, segmentation

237 of the IC from several samples showed that its shape is not uniform and not tetrahedral
238 (Fig. 3B; Supplemental Movie S3 to S7). Most side views, but not all, show triangular
239 faces, while most distal faces are irregularly shaped, and are only triangular-like in a
240 few cases. Hence, the IC in *S. moellendorffii* roots is in general not tetrahedral, and its
241 irregular shape makes it difficult to be recognized, especially in sections that follows
242 only one plane.

243 To confirm this irregular shape of the IC, we also subjected two root samples to
244 serial block face scanning electron microscopy (SBF-SEM), allowing a much higher
245 resolution of the cells and cell walls (Fig. 3, C-J; Supplemental Fig. S1; Supplemental
246 Movie S8 and S9). The ICs seemed to have daughter cells at different faces, with cell
247 plates or young cell walls seen in the mother and the most recent daughter cells
248 (Fig. 3, C and G; Supplemental Fig. S1, A-B and F-G), which suggests that these cells
249 were undergoing or had just finished cell divisions. 3D reconstruction based on the
250 serial sections showed that one IC has five or six faces (face 4 and 5 might be considered
251 as one, see Fig. 3D and Supplemental Fig. S1E), instead of four in a tetrahedron.
252 Furthermore, it has a wedge-like shape with two opposite triangular faces (faces 1 and
253 3) and a rectangular bottom (face 6) (Fig. 3, D-E; Supplemental Fig. S1, C-E,
254 Supplemental Movie S8). The second IC had three major proximal faces (faces 1-3),
255 all with irregular triangular-like shapes, and a pentagonal distal face (face 4) (Fig. 3, H-
256 J; Supplemental Fig. S1, H-J; Supplemental Movie S9). Hence, the ICs are irregular in
257 shape, and not per se having a triangular face in all longitudinal planes. The IC might
258 have this irregular shape as this cell is mitotically active (Fujinami et al., 2017), and
259 therefore the shape changes during intensive cell divisions. This is an important
260 observation to take into consideration when looking for ICs in sections, and explains
261 why it is often troublesome to make a correct designation. By using whole stacks, it is
262 possible to reorient the stack in such a way that ICs are clearly recognizable (as
263 illustrated by the 270 degree view in Fig. 3A), as there always seems to be two faces
264 with a triangular shape.

265 We next sampled root tips during the root branching time course in independent
266 experiments covering different time points. The roots were subjected to whole-mount
267 confocal imaging and stacks were made and segmented to reorient sections and to select
268 planes with clear ICs (Fig. 4). Again, in some roots, two ICs of similar size were
269 positioned next to each other (Fig. 4, A-C; Supplemental Fig. S2, A-C). This further
270 supports the hypothesis for a symmetric division of the IC, which is most probably the
271 first anatomical event leading to root meristem bifurcation.

272 In the absence of genetically encoded markers, live imaging to show that such
273 division indeed results in the formation of two meristems is unfortunately not possible
274 in *S. moellendorffii*. Still, in multiple samples at early time points, we could, based on
275 the cellular pattern, clearly observe that each of the ICs produced their own distal
276 daughter cells in the root cap (Fig. 4, A and B; Supplemental Fig. S2A), indicating that
277 each of these two cells underwent at least one additional formative division to cut off a
278 root cap cell. Furthermore, we also observed multiple root tips in which the two ICs
279 were very close to each other and separated by only one or two layers of short cells
280 (Fig. 4, D-G; Supplemental Fig. S2, D-F). These layers seemed to originate from
281 daughter cells of the new ICs. Based on these observations, it is of high likelihood that
282 the two ICs originally neighbored each other, supporting the hypothesis that
283 dichotomous root branching in *S. moellendorffii* is a result of a symmetric division of
284 the original IC. In this scenario, the two new ICs would each cut off daughter cells in
285 different directions, forming two new meristems (Fig. 4K). These two new meristems
286 or root primordia are initially still embedded in the macroscopically unbranched root,
287 which radially expands because of the doubled meristem (Fig. 4, H-J), but later on grow
288 out to form two branches as described before (Otręba and Gola, 2011).

289 The *S. moellendorffii* Root Branching Transcriptome

290 *Cyclic Gene Expression Profiles Support a Return to the Initial Meristem State*

291 Based on the confocal imaging, almost 40% of the root tips formed two clearly

292 distinguishable new meristems 5 d after the first branching (Fig. 1H), hence we
293 supposed that programs to initiate dichotomous branching mainly occur before this time
294 point. To identify possible molecular mechanisms with a role in root branching
295 initiation in *S. moellendorffii*, we employed the developmental root branching assay for
296 an RNA-seq experiment and sampled root tips on each day from 0 to 5 d after the first
297 branching (time point 0), in which 300-µm apical parts were sampled to enrich for the
298 meristematic region, while non-meristematic root regions were sampled separately
299 (Fig. 5A).

300 Taking into account a fold change (FC) of at least 2 and an adjusted *p*-value (BH
301 FDR corrected) of maximum 0.05, 6601 differentially expressed genes (DEGs) were
302 retrieved between the meristematic and non-meristematic part. 3410 genes were higher
303 expressed in the apical parts and were therefore designated as "meristem-enriched
304 genes". Within the branching time course, however, only 15 genes were differentially
305 expressed with a $|FC| > 2$ (adjusted *p*-value ≤ 0.05; LRT). None of these DEGs had a
306 straightforward annotation (Supplemental Table S1). This low number is not
307 unexpected, as the different root branching samples only differed developmentally and,
308 most likely, in a small region within the same tissue. Differences in gene expression
309 may even only occur in one cell, and hence become diluted within the sampled tips.
310 Still, 1553 genes were significantly (adjusted *p*-value ≤ 0.05; LRT) affected over the
311 branching time course (Fig. 5, B and C; Supplemental Table S1). We therefore
312 designated them provisionally as "root branching genes". Many of these genes were
313 differentially expressed at multiple time points (Fig. 5B; Supplemental Table S1),
314 corroborating a relevant differential expression. Interestingly, the number of DEGs at
315 first steadily increased during the time course and peaked on 2 and 3 d after the first
316 branching, and then decreased towards the end of the time course (Fig. 5C). Hence,
317 the final state showed less differential expression and was more similar to the original
318 state.

319 To get a better insight into the expression profiles, the 1553 "root branching genes"

320 were subjected to a cluster analysis via WGCNA (Langfelder and Horvath, 2008). The
321 analysis revealed 22 main expression profiles (Fig. 5D), which we further grouped
322 according to their shapes. As such, the clusters could be classified into four major
323 groups: we designated the transiently upregulated and downregulated gene clusters as
324 "Dome" (further grouped into Early peak, Late peak and Broad peak subgroups) and
325 "Valley", respectively; constitutively upregulated and downregulated clusters were
326 named "Up" and "Down", respectively; only a few genes could not be classified into
327 any one of these groups (Fig. 5D). Overall, the majority of genes clustered in the Dome
328 (490/1553) or the Valley (560/1553) groups, which fits the decreased number of DEGs
329 towards the end of the time course.

330 In summary, both the number of DEGs per time point and the clustering of the
331 expression profiles support a generally cyclic expression pattern, which might be
332 correlated with developments at the cellular level: a starting state with a single meristem
333 that rapidly initiates bifurcation, or evolves into an early bifurcation state and then
334 evolves again into two separated single meristems resembling the initial state.

335 ***Root Branching Transcriptome to Identify Core Meristem-Enriched Genes***

336 The Selaginella root branches in association with the development of two root
337 meristems. Therefore, especially at an early stage with two meristems, we expected
338 meristem genes to be differentially expressed: when the meristem bifurcates, transcripts
339 of genes specifically expressed, or repressed, in the IC or in its neighborhood, would
340 be relatively more, or less, abundantly present. Indeed, at an early stage, two young
341 meristems are present within a non-expanded root tip. When the two meristems and the
342 root tip enlarge (Fig. 4), this abundance would get diluted and evolve towards the end
343 of the time course to a relative expression level as in a non-bifurcated meristem. Within
344 the 1553 "root branching genes", 452 out of the 3410 meristem-enriched genes were
345 present (Supplemental Table S1), and hence, while this is still an overrepresentation
346 (Fig. 6, A-C; Supplemental Table S2), a big portion of the meristem-enriched genes
347 were not differentially expressed during meristem bifurcation. We presume that the

348 group of "meristem-enriched genes" as such might still encompass many genes that do
349 not associate with the meristem itself, but with another part of the root tip. The other
350 possibility that these genes might be associated with maintaining meristem identity and
351 therefore are not differentially expressed during bifurcation cannot be excluded. Still,
352 especially meristem-enriched genes that are differentially expressed during the root
353 branching time course ("root branching genes") (Fig. 6, A and B), are expected to be
354 associated with the root meristem function and might be of special interest.

355 We were intrigued by the overrepresentation of meristem genes in the
356 downregulated root branching DEGs, which showed a 1.9-fold overrepresentation in
357 meristem genes (Fig. 6C), which could point to a loss of meristem identity or meristem
358 activity during the bifurcation process. In the GO, InterPro and MapMan term
359 enrichment analyses of this group, we noticed some terms related to microtubule-
360 binding, cytoskeleton or cell division, including Heat Shock Protein 90-, Elongation
361 Factor-, and kinesin-related terms (Krtková et al., 2012; Zhu and Dixit, 2012; Krtková
362 et al., 2016), but also "microtubule binding", "cytokinesis" and "cell cycle"
363 (Supplemental Table S3). Indeed, a lot of cell cycle-related genes could be found in the
364 top downregulated meristem-enriched genes, including extensin, callose synthase and
365 phragmoplast-related *KINESIN-LIKE* (*KIN*) genes (Supplemental Table S1). When
366 taking into account the top meristem-enriched genes in this subset, in particular KIN7,
367 10, 12 and 14 proteins were found (Fig. 6D), known to be associated with phragmoplast
368 formation or orientation, and hence involved in cell plate formation and cell division
369 (Zhu and Dixit, 2012). Thus, the group of downregulated meristem-genes were mainly
370 related to cell division, which points to an arrest or inhibition of cell divisions during
371 root branching. A more detailed analysis showed that these genes were especially
372 present and enriched in Down clusters (137 genes) or in the big Valley-0 cluster (117
373 genes) (Fig. 6C; Supplemental Table S2). These clusters in general showed a middle to
374 late downregulation, which is also notable on the general expression profile of these
375 genes (Fig. 6, B and D). Possibly, cell divisions in the original meristem stopped or at

376 least decreased, while daughter cells of the two new ICs took over the meristem activity
377 towards the end of the time course.

378 The 173 of the meristem-enriched root branching genes that showed an
379 upregulation in the root branching time course might be of interest. These genes were
380 especially present and enriched in the early responsive (Early peak) Dome cluster,
381 showing an expression profile that went up relatively early during the branching course,
382 but returned to the basal level again at the end (Fig. 5D). Therefore, these clusters also
383 show a much higher overrepresentation of meristem-enriched genes (Fig. 6C). The
384 early upregulation of these genes indicates that two young meristems were formed early,
385 which then matured towards the end of the branching time course.

386 To get insights into the function of the 173 meristem-enriched genes that were
387 upregulated during the branching, GO, InterPro and MapMan term enrichment analyses
388 were performed. These analyses clearly showed an enrichment in terms related to cell
389 growth, and more particularly, in ribosome- and translation-related terms (Fig. 6E;
390 Supplemental Table S3). The gene set indeed included a broad range of ribosomal
391 proteins (Supplemental Table S1). Interestingly, such genes or terms are typically
392 enriched in young meristematic angiosperm root cells as well. For example,
393 Arabidopsis single-cell transcriptomic studies showed that ribosomal protein-encoding
394 genes are enriched in meristematic clusters (Ryu et al., 2019; Shulse et al., 2019; Zhang
395 et al., 2019). Hence, the 173 genes seemed to be associated with young meristematic
396 cells, underlining and validating the value of the root branching dataset to select core-
397 meristem genes.

398 Thus, this set can be used to highlight genes with a putative role in the *S.*
399 *moellendorffii* root meristem, especially as the subset of 173 genes are probably
400 differentially expressed in the young meristem, possibly even in the IC, but not in the
401 root cap or other regions of the root tip.

402 We queried the 173 genes for orthologs of genes encoding better characterized
403 proteins in Arabidopsis. This subset contains, besides many ribosomal proteins, an

404 *ARABIDOPSIS RESPONSE REGULATOR15* (*ARR15*) ortholog (SMO274G0055) and
405 an *AUXIN RESPONSE FACTOR7* (*ARF7*) ortholog (SMO361G0080). *ARR15*,
406 negatively regulating cytokinin signaling, is important for stem cell specification in the
407 Arabidopsis root meristem (Müller and Sheen, 2008), and the auxin-induced *ARF7* is
408 important during LR initiation, leading to a new root meristem (Okushima et al., 2005).
409 Their presence in this set of genes suggests a possible importance of the two genes in
410 *S. moellendorffii* root meristem establishment or maintenance as well, and as such a,
411 possibly partially, in the conserved genetic program of root stem cell specification.

412 ***Candidate Regulators of Dichotomous Root Branching***

413 To further identify possible regulators in the root branching process, we queried all
414 1553 root branching genes for transcription factors and orthologs of genes with well-
415 described roles in *Arabidopsis* root meristem maintenance or LR branching, including
416 auxin and cytokinin signaling genes, receptor kinases and cell cycle genes
417 (Supplemental Table S5). Transcription factors were collected via PlantTFDB v5 (Tian
418 et al., 2019). As we noticed that not all ARF and ARR transcription factors were
419 recognized in the PlantTFDB, we also looked for their orthologs and included them in
420 the transcription factor query (Supplemental Table S5).

421 Among these possible regulators, 40 were differentially expressed during the root
422 branching time course (Fig. 7A), and might be involved in the regulation of
423 dichotomous root branching. These included four auxin-responsive *ARF* genes, two
424 cytokinin-regulating *ARR* genes, and orthologs of the auxin transporter *PIN2*, the
425 cytokinin-responsive *CYTOKININ RESPONSE FACTOR1* (*CRF1*), the cytokinin
426 receptor *AHK2*, the gibberellic acid signaling gene *REPRESSOR OF GA-LIKE1*
427 (*RGL1*), the ethylene signaling gene *ETHYLENE-INSENSITIVE3-LIKE1* (*EIL1*) and
428 the brassinosteroid signaling gene *BES1/BZR1 HOMOLOGUE4* (*BEH4*). The presence
429 of these genes might indicate a role of hormonal signaling in a very complex way in
430 dichotomous root branching and the associated meristem maintenance.

431 We also noticed the presence of homologs of both *TARGET OF MONPTEROS5*

432 (*TMO5*) and *LONESOME HIGHWAY* (*LHW*). In Arabidopsis, the two form a dimer and
433 are together crucial for vasculature initiation (De Rybel et al., 2013; De Rybel et al.,
434 2014). This control is shown to be highly conserved in all vascular plants (Lu et al.,
435 2020). In Arabidopsis, the two transcription factors have a different spatial expression
436 pattern and overlap at the vascular domain (De Rybel et al., 2013). Within the *S.*
437 *moellendorffii* root branching course, *LHW* was early downregulated, but reached its
438 basal level again at the end, whereas *TMO5* was upregulated in particular at the end
439 (Fig. 7A). Hence, the *LHW* and *TMO5* homologs showed a common high expression
440 level towards to the end of our time course (from 3 and 5 d), when two young meristems
441 were present, possibly indicating increased vascular development at that stage.

442 Interestingly, only a few transcription factor-encoding DEGs showed an early
443 upregulation. In particular, a *WUSCHEL RELATED HOMEOBOX* (*WOX*)
444 (SMO239G0078) and a *SCARECROW* (*SCR*) (SMO358G0343) homolog, both
445 important and transcriptionally interacting stem cell regulators (Shimotohno et al., 2018;
446 Motte et al., 2020), showed a strong early induction (Fig. 7A) and are highly co-
447 expressed (Fig. 7B). Possibly, these were involved in the control of dichotomous root
448 branching. Interestingly, also *RBR1* (SMO134G0004), important in stem cell fate
449 decision as well and a negative interactor of *SCR* (Cruz-Ramírez et al., 2012), was
450 found in the list. As shown for Arabidopsis, *RBR1* interacts with E2F transcription
451 factors (Wildwater et al., 2005), of which a homolog, SMO133G0001 was also
452 differentially expressed in our dataset. Noteworthy, at least in Arabidopsis, *RBR1* and
453 *E2F3* show a high degree of co-expression (Magyar et al., 2012), which we also
454 observed in the *S. moellendorffii* root branching time course (Fig. 7B).

455 In contrast to the Dome expression profile of the *WOX* and *SCR* homologs, we
456 observed a downregulating Valley profile for the *S. moellendorffii RBR1* and *E2F3*
457 homologs. The two group of genes thus showed an inversely correlated expression
458 pattern (Fig. 7B), which intriguingly fits within the pathway model proposed for
459 Arabidopsis.

460 **DISCUSSION**

461 Lycophyte roots branch dichotomously due to bifurcation of the apical meristem.
462 Activities of the IC have been assumed to play a key role in this process, especially in
463 branching initiation, whereas it remained unclear how its cellular activities are
464 associated with root bifurcation in the lycophyte *S. moellendorffii*. Previous reports on
465 Selaginella root bifurcation suggested that the single root apical IC undergoes
466 segmentation and becomes indistinguishable, which is followed by the initiation of two
467 new ICs at the flanks and the formation of two new root meristems (Imaichi and Kato,
468 1989; Otręba and Gola, 2011). Barlow and Lück (2004) hypothesized that, after a set
469 of rigid cell divisions, a derivative of the IC becomes a new IC to form the second root
470 meristem. In contrast, our results point out that root bifurcation starts with a symmetric
471 division of the original IC, which gives rise to two new ICs. Such a symmetric division
472 to initiate dichotomous root branching in Selaginella has never been reported.
473 Additionally, it was stated that a longitudinal symmetric division of a tetrahedral cell is
474 unlikely to occur, because the surface area of the inserted cell wall is relatively big and
475 would be inefficient (Cooke and Paolillo Jr, 1980; Gola, 2014). However, we showed
476 that the IC is irregular and possibly changing in shape, and in general not tetrahedral.
477 As such, ICs might acquire geometries that are better suited to undergo a symmetric
478 division.

479 Still, there could be other factors controlling the IC to undergo the symmetric
480 division to initiate dichotomous root branching. As the stem cell is surrounded by
481 multiple cells in the meristem, interactions and feedbacks from the neighboring cells
482 may also contribute to the first division initiating root branching in land plants. In
483 Arabidopsis, the auxin reflux from surrounding endodermal cells allows auxin
484 accumulation in the founder cells for transition to LR initiation (Dubrovsky et al., 2008;
485 Marhavý et al., 2013; Cavallari et al., 2021), also showing a critical role of auxin in the
486 control of the first asymmetric division. However, we detected differential
487 downregulation of multiple auxin-responsive *ARF* genes in the branching time course,

488 suggesting a reduction in the auxin response during the process. Thus, auxin is not likely
489 to accumulate in the IC to induce the first symmetric division. Supportive for this, we
490 earlier found that Selaginella root branching is not induced by auxins (Fang et al., 2019).
491 Moreover, a spatial accommodation by neighboring cells, which may involve
492 mechanical forces, is also essential for Arabidopsis LR initiation. Specifically, pericycle
493 cells swell before the first asymmetric division, which is actively accommodated by the
494 neighbor endodermis (Vermeer et al., 2014; Vermeer and Geldner, 2015; Ramakrishna
495 et al., 2019). However, it is totally unknown whether the IC and the neighboring
496 derivatives need to undergo any morpho-cytological alteration to promote root
497 branching initiation in Selaginella.
498 During Arabidopsis root growth, (lateral) root branching formation takes place
499 periodically: protoxylem cells in the basal meristem undergo temporal oscillations in
500 auxin concentrations and auxin-responsive gene expression levels, which allows these
501 cells to transport these priming signals to the pericycle cells, which also get primed,
502 forming competent sites to initiate LRs (De Smet et al., 2007; Moreno-Risueno et al.,
503 2010; Van Norman et al., 2014; Xuan et al., 2016; Laskowski and ten Tusscher, 2017).
504 In Selaginella, roots also branch repetitively but dichotomously (Fang et al., 2019),
505 which coincides with a generally cyclic gene expression profile. Possibly, this involves
506 priming signals as well, which may be included in our dataset.
507 It has been hypothesized that lycophyte roots have a shoot origin (Gensel et al.,
508 2001), which should result in shared developmental mechanisms between the shoot and
509 root meristem. This was for instance shown in the lycophyte Lycopodium, where
510 bifurcation of both meristems starts with the emergence of mitotically active cells in a
511 similar quiescent region (Fujinami et al., 2021). In contrast, Selaginella bifurcation of
512 the shoot meristem begins with a symmetric division of the IC (Christopher and Andrew,
513 2009).This fits our observation of the same division in the root, and corroborates the
514 shoot origin of the root in lycophytes. It also underlines the possible differences in root
515 anatomy and bifurcation mechanisms, as not all lycophyte subclades have single ICs,

516 and supports along with the fossil record that roots originated multiple times during the
517 evolution of lycophytes (Gensel et al., 2001; Fujinami et al., 2017; Fujinami et al., 2020;
518 Hetherington et al., 2021).

519 Although roots originated multiple times during evolution, it is hypothesized based
520 on comparative transcriptomics studies that a common rootless ancestor of vascular
521 plants possessed an inheritable genetic tool kit that descendants recruited for similar
522 root meristem-related biological processes, resulting in a highly conserved root
523 developmental program within vascular plants (Huang and Schiefelbein, 2015; Ferrari
524 et al., 2020). Details on this conserved genetic program are lacking, but using a root
525 branching time course in *S. moellendorffii*, we succeeded to introduce specific core-
526 meristem genes and showed the presence of multiple homologs of Arabidopsis genes
527 with a known role in meristem establishment. This further corroborates that the genetic
528 control of root development, despite morphological differences, is indeed highly
529 conserved and further supports the parallel recruitment of an, at least partial, common
530 genetic program.

531 As the organization of the Selaginella root meristem is less complex than that of
532 seed plants, a more elementary pathway controlling stem cell fate decisions may be
533 presumed (Motte et al., 2020). Thus, it might be anticipated that Selaginella requires a
534 more limited set of genetic players to install and maintain the stem cell. We identified
535 homologs of some known root stem cell controllers in Arabidopsis, including, *WOX*,
536 *SCR*, *RBR1* and *E2F3*-family members, as the candidate regulators of dichotomous root
537 branching in Selaginella. Moreover, we found that their expression profiles fit within
538 the pathway model in Arabidopsis. Hence, conserved pathways, involving SCR-
539 dependent regulation of a *WOX* gene and a RBR1-SCR feedback loop for stem cell fate
540 decisions, or at least roles of *RBR1* and *E2F3* similar as those of the Arabidopsis root
541 (Wildwater et al., 2005; Stahl et al., 2009; Cruz-Ramírez et al., 2012), could be
542 speculated. It is important to note that WOX functioning in angiosperm stem cell
543 control and its action via transcriptional repression is restricted to the WUS subclade

544 (Dolzblasz et al., 2016; Zhou et al., 2018), which is not present in *S. moellendorffii* (Wu
545 et al., 2019). Thus, the presence of *WOX* as a branching DEG may imply a different
546 mechanism, possibly as a transcriptional activator (Motte et al., 2020). It is tempting to
547 hypothesize that these genes are the central components in the evolutionarily early
548 pathways controlling the IC, and were recruited for both dichotomous and LR
549 branching formation.

550 Overall, we generated a relevant dataset, in which multiple candidate regulators of
551 root meristem bifurcation in *S. moellendorffii* could be identified that possibly show
552 high conservation with similar pathways in seed plants. In contrast to existing *S.*
553 *moellendorffii* datasets, which mainly focused on tissue-specific expression, we here
554 characterized expression patterns during a developmental process in which new (root)
555 stem cells are established. Although the molecular research using *S. moellendorffii* is
556 still at its infancy, this dataset can be a useful resource to identify possible root
557 meristem- and stem cell-related Selaginella or lycophyte genes. Due to the pioneering
558 evolutionary position of this lineage during plant colonization of land, this resource can
559 be very useful to identify conserved and early (root) stem cell regulators, and to unravel
560 the early pathways that were at the base of pluripotency.

561 MATERIALS AND METHODS

562 Plant Materials

563 *S. moellendorffii* plants were obtained from the lab of Jo Ann Banks, Purdue
564 University. Plants were grown aseptically under a 16-h light/8-h dark photoperiod at
565 20.25–43.2 μmol/m^2/s in a 24°C growth chamber and roots developed after the transfer
566 of explants to fresh medium as previously reported (Fang et al., 2019).

567 Microscopy

568 To track root branching events, roots were observed daily starting from their
569 appearance on rhizophores using a Leica S9I stereomicroscope.

570 For whole-mount confocal imaging, *S. moellendorffii* root tips were first fixed in
571 50% methanol and 10% acetic acid, and then subjected to modified pseudo-Schiff
572 propidium iodide (mPS-PI) staining described by Truernit et al. (2008). Confocal
573 imaging was performed using a Zeiss LSM 5 Exciter microscope (25x water immersion
574 objective lens) with an argon ion laser at 488/505 nm as the excitation/emission
575 wavelengths, or a Leica SP2 confocal microscope [63x water corrected objective (NA
576 1.2) lens and pinhole = 1 AU] with an argon ion laser at 514/600-650 nm as the
577 excitation/emission wavelengths. Alternatively, modified staining was performed with
578 a small change in the composition of chloral hydrate solution [8 g chloral hydrate, 3
579 mL glycerol, and 1 mL water (8:3:1)]. Z-stacks were taken for all samples to allow
580 collective detection of the meristematic region present at different planes. A subset of
581 samples, including the ones used for segmentation, were after fixation subjected to
582 amylase treatment in order to digest starch granules. Root tips were washed three times
583 with water and subsequently treated overnight with α-amylase at a concentration of 300
584 U/ml in a buffer containing 20 mM phosphate pH 7.0, 2mM NaCl, 0.25 mM Ca_2Cl.
585 Samples were then washed with water and fixed again in 50% methanol and 10% acetic
586 acid for 1 h. Samples were subsequently washed two times with 1X PBS and transferred
587 to ClearSee solution (Kurihara et al., 2015) and gently stirred for 1 week. Finally, the
588 samples were stained for 1 h in ClearSee solution containing 0.1% Calcofluor White
589 and were washed afterwards for 30 min in ClearSee solution before imaging. Confocal
590 imaging of the Calcofluor White stained roots was conducted using 405 nm excitation
591 and 425-475 nm wavelength detection using a Leica SP8X system. Confocal stacks
592 generated for segmentation were imaged using a 63X water-corrected objective (NA of
593 1.2) and a pinhole of 0.6 AU. Stacks were further processed using MorphoGraphX
594 (Barbier de Reuille et al., 2015) to identify ICs and to obtain clear sections showing the
595 meristematic organization.
596 For histological sections, root tip samples were fixed in 1% glutaraldehyde and 4%
597 paraformaldehyde, followed by dehydration and embedding in Technovit 7100 resin

598 (Heraeus Kulzer) according to the manufacturer's instruction. Transparent strips were
599 used to orient tissues for proper orientation (Beeckman and Viane, 2000). 2-µm sample
600 sections were cut using a Leica Reichert-Jung 2040 Autocut Microtome, dried on object
601 glasses using a hot plate (20–40 °C), stained for cell walls with 0.05% toluidine blue or
602 ruthenium red (Acros Organics) for 10 min and then rinsed with water to wash off
603 excess dyes. The sections were then mounted in Depex medium (Sigma) and covered
604 with cover slips for observation and photography using an Olympus BX53 microscope.
605 For serial block face scanning electron microscopy (SBF-SEM), samples were
606 fixed using 2% paraformaldehyde and 2.5% glutaraldehyde in 0.1 M Sodium
607 Cacodylate pH 7.4. Next, samples were processed en-bloc using a ROTOTO staining
608 as described previously (Fendrych et al., 2014). Finally, resin-embedded root tips were
609 mounted on aluminum specimen pins (Melotte) using conductive epoxy (Circuit
610 Works), and coated with 5 nm of Pt in a Quorum sputter coater. Next, samples were
611 placed in the Gatan 3View 2XP in a Zeiss Merlin SEM, for imaging at 1.6 kV using the
612 Gatan Digiscan II BSED detector. The system was set up to automatically take 1000
613 images at a pixel-size of 15 nm, cutting 100-nm sections of the block-face between each
614 image, resulting in a volume of 150 x 150 x 100 µm.
615 For registration of the 3D image stack, IMOD (http://bio3d.colorado.edu/imod/)
616 was used. Orthogonal views were obtained in Fiji (http://fiji.sc/Fiji). Segmentation was
617 done using Microscopy Image browser (http://mib.helsinki.fi/) and rendering was done
618 using Imaris (Bitplane).

619 **Extraction of Initial Cell Geometry**

620 Extraction of initial cell geometry was performed using MorphoGraphX (Barbier
621 de Reuille et al., 2015). Confocal images were prepared for segmentation using a
622 Gaussian blur of 0.5 in the X, Y and Z directions. Segmentation was performed using
623 the ITK watershed auto seeded algorithm with a threshold of 800 and segmentation
624 errors were manually corrected. 3D cell meshes were constructed for the region of the
625 root containing the IC, using the process marching cubes 3D with a cube size of 0.5,

626 and 50 smooth passes at the time of mesh generation to minimize alterations to the mesh
627 structure (Bassel, 2015). All other cells in the mesh were then deleted to isolate the IC,
628 which was subject to a further 5 smooth passes using the smooth mesh tool to facilitate
629 qualitative visualization.

630 **RNA-Seq**

631 Sampled roots in the time course (300 root tips per sample, 4 biological repeats per
632 time point) were cut off using a pair of stainless microscissors and then stored in
633 RNA*later*® RNA Stabilization Solution (Thermo Fisher Scientific) according to the
634 manufacturer's instruction. Subsequently, microdissection was performed to collect
635 root apices of 0.3 mm long, as well as non-meristematic regions between apices and
636 branching point for the 5 d post first branching samples. The samples were then
637 collected in 2-mL RNase-free Eppendorf tubes with an RNase-free metal ball [diameter:
638 5 mm, sprayed by RNaseZap™ RNase Decontamination Solution (Invitrogen™,
639 Thermo Fisher Scientific)] and frozen in liquid nitrogen. After collection, samples were
640 stored at -70 °C.

641 For RNA extraction, samples were ground three times using a QIAGEN Retsch
642 Tissuelyser (30 Hz, 30 s). RNA extraction was done via TRIzol™ reagent (Thermo
643 Fisher Scientific) and the RNeasy Plant Mini Kit (Qiagen) according to the provided
644 protocols.

645 RNA concentration and purity were determined spectrophotometrically using a
646 Nanodrop ND-1000 (Nanodrop Technologies) and RNA integrity was assessed using a
647 Bioanalyzer 2100 (Agilent). Per sample, an amount of 250 ng of total RNA was used
648 as input. Using the Illumina TruSeq Stranded mRNA Sample Prep Kit (protocol version:
649 Part # 15031047 Rev. E - October 2013), poly-A containing mRNA molecules were
650 purified from the total RNA input using poly-T oligo-attached magnetic beads. In a
651 reverse transcription reaction using random primers, RNA was converted into first
652 strand cDNA and subsequently converted into double-stranded cDNA in a second
653 strand cDNA synthesis reaction using DNA PolymeraseI and RNAse H. The cDNA

654 fragments were extended with a single 'A' base to the 3' ends of the blunt-ended cDNA
655 fragments after which multiple indexing adapters were ligated introducing different
656 barcodes for each sample. Finally, enrichment PCR was carried out to enrich those DNA
657 fragments that have adapter molecules on both ends and to amplify the amount of DNA
658 in the library. Sequence-libraries of each sample were equimolarly pooled and
659 sequenced on Illumina HiSeq 4000 (SBS 300 cycles, Paired End Reads:151-8-8-151)
660 at the VIB Nucleomics Core (www.nucleomics.be).
661

662 **Expression Analysis**

663 We used two versions of *S. moellendorffii* annotated genomes: the NCBI version
664 (Annotation Release 100, released in 2018, containing 33,283 genes) and the JGI
665 version (v1.0, released in 2007, containing 22,285 genes). While the former is the most
666 recent, and based on transcriptome data more correctly mapped, the JGI version is more
667 widely used in bioinformatic tools. Therefore, we performed the mapping/alignment
668 based (i) on NCBI if there was a 1:1 BLAST hit between NCBI and JGI annotations
669 (and including the corresponding JGI identifiers), and (ii) on JGI for genes that were
670 uniquely present in the JGI annotation. Counts were quantified using Salmon (Patro et
671 al., 2017) and normalization was done using the DESeq2 R package (Love et al., 2014).
672 To correct for the batch effect, Limma (Ritchie et al., 2015) was applied.

673 Differential analyses of the count data were performed using DESeq2 (Love et
674 al., 2014), only considering normalized read counts ≥ 10. PCA was used to identify and
675 omit outliers within the biological repeats and differential gene expression was analysed
676 using a multiple factor analysis (MFA).The expression during branching was assessed
677 by a likelihood-ratio test (LRT) (Supplemental Table S1). Differentially expressed
678 genes were selected based on an adjusted *p*-value [Benjamini & Hochberg (BH)
679 (Benjamini and Hochberg, 1995) false discovery rate (FDR) corrected] ≤ 0.05. In
680 addition, meristem DEGs were only retained in case of a |FC| ≥ 2. Heatmaps showing
681 expression profiles were generated using the R package "pheatmap". Weighted gene co-

682 expression network analysis (WGCNA) was performed according to Langfelder and
683 Horvath (2008) in the pipeline of DESeq2.

684 Statistical significance of the overlap between two groups of genes was calculated
685 via the Fisher exact test. Representation factors were calculated by dividing the number
686 of overlapping genes by the number of expected genes in the overlap.

687 Data for Gene Ontology (GO), InterPro and Mapman term enrichment were
688 computed using the 'Workbench' function of the Dicots PLAZA tool version 4.5:
689 https://bioinformatics.psb.ugent.be/plaza/versions/plaza_v4_5_dicots/ (Vandepoele et
690 al., 2013; Van Bel et al., 2018), with default settings.

691 Homology or orthology between Arabidopsis and *S. moellendorffii* genes was
692 based on the gene families in the Dicots PLAZA version 4.5.

693 RNA-seq data are available in the ArrayExpress database
694 (https://www.ebi.ac.uk/arrayexpress) under the accession number XXXX.

695 Supplemental Data

696 The following supplemental materials are available.

697 **Supplemental Figure S1.** Additional SBF-SEM images and proximal views of the
698 reconstructed root ICs in *S. moellendorffii*.

699 **Supplemental Figure S2.** Additional confocal images taken during the root
700 branching assay in *S. moellendorffii.*

701 **Supplemental Movie S1.** *S. moellendorffii* shoot explant with root formation that
702 repetitive bifurcation of the roots.

703 **Supplemental Movie S2.** Confocal stack of an unbrached *S. moellendorffii* root.

704 **Supplemental Movie S3.** First IC in Figure 3B.

705 **Supplemental Movie S4.** Second IC in Figure 3B.

706 **Supplemental Movie S5.** Third IC in Figure 3B.

707 **Supplemental Movie S6.** Fourth IC in Figure 3B.

708 **Supplemental Movie S7.** Fifth IC in Figure 3B.

709 **Supplemental Movie S8.** IC in Figure 3D-F.

710 **Supplemental Movie S9.** IC in Figure 3H-J.

711 **Supplemental Table S1:** Processed RNA-Seq gene expression values.

712 **Supplemental Table S2:** Overlap of genes between different subsets or clusters
713 and the meristem-enriched genes.

714 **Supplemental Table S3:** GO, Mapman and Interpro terms associated with the
715 meristem-enriched genes that were downregulated in the root branching course.

716 **Supplemental Table S4:** GO, Mapman and Interpro terms associated with the
717 meristem-enriched genes that were upregulated in the root branching course.

718 **Supplemental Table S5:** Selaginella orthologs or homologs from lateral root or
719 root stem cell related gene families as retrieved from PLAZA version 4.5
720 (https://bioinformatics.psb.ugent.be/plaza/versions/plaza_v4_5_dicots/).

721 ## ACKNOWLEDGMENTS

722 We thank Lieven Sterck and Ignacio Eguinoa for support in bioinformatic analyses,
723 Anna Kremer, Benjamin Pavie, Peter Borghgraef and Saskia Lippens for assistance and
724 guidance with the SBF-SEM, Davy Opdenacker for technical support and Annick Bleys
725 for help in preparing the mansucript. We also would like to thank Moritz Nowack, Edyta
726 Gola and Koen Geuten for the helpful discussions and comments on the manuscript.

727

728 ## References

729 **Banks JA** (2009) Selaginella and 400 million years of separation. Annu Rev Plant Biol
730 **60:** 223-238

731 **Banks JA, Nishiyama T, Hasebe M, Bowman JL, Gribskov M, dePamphilis C,**
732 **Albert VA, Aono N, Aoyama T, Ambrose BA, et al** (2011) The Selaginella
733 genome identifies genetic changes associated with the evolution of vascular
734 plants. Science **332:** 960-963

735 **Barbier de Reuille P, Routier-Kierzkowska A-L, Kierzkowski D, Bassel GW,**
736 **Schüpbach T, Tauriello G, Bajpai N, Strauss S, Weber A, Kiss A, et al** (2015)

737 MorphoGraphX: A platform for quantifying morphogenesis in 4D. eLife **4:**
738 e05864
739 **Barlow PW, Lück J** (2004) Deterministic cellular descendance and its relationship to
740 the branching of plant organ axes. Protoplasma **224:** 129-143
741 **Bassel GW** (2015) Accuracy in quantitative 3D image analysis. The Plant Cell **27:** 950-
742 953
743 **Beeckman T, Viane R** (2000) Embedding thin plant specimens for oriented sectioning.
744 Biotech Histochem **75:** 23-26
745 **Benjamini Y, Hochberg Y** (1995) Controlling the false discovery rate - a practical and
746 powerful approach to multiple testing. J R Stat Soc Ser B - Stat Methodol **57:**
747 289-300
748 **Cavallari N, Artner C, Benkova E** (2021) Auxin-regulated lateral root organogenesis.
749 Cold Spring Harb Perspect Biol **13:** a039941
750 **Christopher SJ, Andrew ND** (2009) The developmental pattern of shoot apices in
751 *Selaginella kraussiana* (Kunze) A. Braun. Int J Plant Sci **170:** 1009-1018
752 **Cooke TJ, Paolillo Jr DJ** (1980) The control of the orientation of cell divisions in fern
753 gametophytes. Am J Bot **67:** 1320-1333
754 **Crombez H, Roberts I, Vangheluwe N, Motte H, Jansen L, Beeckman T, Parizot B**
755 (2016) Lateral root inducible system in Arabidopsis and maize. J Vis Exp **(107):**
756 e53481
757 **Cruz-Ramírez A, Díaz-Triviño S, Blilou I, Grieneisen Verônica A, Sozzani R,**
758 **Zamioudis C, Miskolczi P, Nieuwland J, Benjamins R, Dhonukshe P, et al**
759 (2012) A bistable circuit involving SCARECROW-RETINOBLASTOMA
760 integrates cues to inform asymmetric stem cell division. Cell **150:** 1002-1015
761 **De Rybel B, Adibi M, Breda AS, Wendrich JR, Smit ME, Novák O, Yamaguchi N,**
762 **Yoshida S, Van Isterdael G, Palovaara J, et al** (2014) Integration of growth
763 and patterning during vascular tissue formation in *Arabidopsis*. Science **345:**
764 1255215

765 **De Rybel B, Möller B, Yoshida S, Grabowicz I, de Reuille PB, Boeren S, Smith RS,**
766 **Borst JW, Weijers D** (2013) A bHLH complex controls embryonic vascular
767 tissue establishment and indeterminate growth in Arabidopsis. Dev Cell **24:**
768 426-437
769 **De Rybel B, Vassileva V, Parizot B, Demeulenaere M, Grunewald W, Audenaert D,**
770 **Van Campenhout J, Overvoorde P, Jansen L, Vanneste S, et al** (2010) A
771 novel Aux/IAA28 signaling cascade activates GATA23-dependent specification
772 of lateral root founder cell identity. Curr Biol **20:** 1697-1706
773 **De Smet I, Tetsumura T, De Rybel B, Frei dit Frey N, Laplaze L, Casimiro I,**
774 **Swarup R, Naudts M, Vanneste S, Audenaert D, et al** (2007) Auxin-
775 dependent regulation of lateral root positioning in the basal meristem of
776 *Arabidopsis*. Development **134:** 681-690
777 **De Smet I, Vassileva V, De Rybel B, Levesque MP, Grunewald W, Van Damme D,**
778 **Van Noorden G, Naudts M, Van Isterdael G, De Clercq R, et al** (2008)
779 Receptor-like kinase ACR4 restricts formative cell divisions in the *Arabidopsis*
780 root. Science **322:** 594-597
781 **Dolzblasz A, Nardmann J, Clerici E, Causier B, van der Graaff E, Chen J, Davies**
782 **B, Werr W, Laux T** (2016) Stem cell regulation by *Arabidopsis WOX* genes.
783 Mol Plant **9:** 1028-1039
784 **Dubrovsky JG, Sauer M, Napsucialy-Mendivil S, Ivanchenko MG, Friml J,**
785 **Shishkova S, Celenza J, Benková E** (2008) Auxin acts as a local
786 morphogenetic trigger to specify lateral root founder cells. Proc Natl Acad Sci
787 USA **105:** 8790-8794
788 **Fang T, Motte H, Parizot B, Beeckman T** (2019) Root branching is not induced by
789 auxins in *Selaginella moellendorffii*. Front Plant Sci **10:** 154
790 **Fang T, Motte H, Parizot B, Beeckman T** (2021) Early "rootprints" of plant
791 terrestrialization: Selaginella root development sheds light on root evolution in
792 vascular plants. Front Plant Sci **12:** 735514

793 **Fendrych M, Van Hautegem T, Van Durme M, Olvera-Carrillo Y, Huysmans M,**
794 **Karimi M, Lippens S, Guérin CJ, Krebs M, Schumacher K, et al** (2014)
795 Programmed cell death controlled by ANAC033/SOMBRERO determines root
796 cap organ size in *Arabidopsis*. Curr Biol **24:** 931-940
797 **Ferrari C, Shivhare D, Hansen BO, Pasha A, Esteban E, Provart NJ, Kragler F,**
798 **Fernie A, Tohge T, Mutwil M** (2020) Expression atlas of *Selaginella*
799 *moellendorffii* provides insights into the evolution of vasculature, secondary
800 metabolism, and roots. Plant Cell **32:** 853-870
801 **Fujinami R, Nakajima A, Imaichi R, Yamada T** (2021) *Lycopodium* root meristem
802 dynamics support homology between shoots and roots in lycophytes. New
803 Phytol **229:** 460-468
804 **Fujinami R, Yamada T, Imaichi R** (2020) Root apical meristem diversity and the
805 origin of roots: insights from extant lycophytes. J Plant Res **133:** 291-296
806 **Fujinami R, Yamada T, Nakajima A, Takagi S, Idogawa A, Kawakami E, Tsutsumi**
807 **M, Imaichi R** (2017) Root apical meristem diversity in extant lycophytes and
808 implications for root origins. New Phytol **215:** 1210-1220
809 **Gensel PG, Kotyk ME, Basinger JF** (2001) Morphology of above- and below-ground
810 structures in Early Devonian (Pragian-Emsian) plants. *In* PG Gensel, D
811 Edwards, eds, Plants invade the land: Evolutionary and environmental
812 perspectives. Columbia University Press, New York, USA, pp 83-102
813 **Gola EM** (2014) Dichotomous branching: the plant form and integrity upon the apical
814 meristem bifurcation. Front Plant Sci **5:** 263
815 **Hao S, Xue J, Guo D, Wang D** (2010) Earliest rooting system and root : shoot ratio
816 from a new *Zosterophyllum* plant. New Phytol **185:** 217-225
817 **Herrbach V, Chirinos X, Rengel D, Agbevenou K, Vincent R, Pateyron S, Huguet**
818 **S, Balzergue S, Pasha A, Provart N, et al** (2017) Nod factors potentiate auxin
819 signaling for transcriptional regulation and lateral root formation in *Medicago*
820 *truncatula*. J Exp Bot **68:** 569-583

821 **Hetherington AJ, Berry CM, Dolan L** (2020) Multiple origins of dichotomous and
822 lateral branching during root evolution. Nat Plants **6:** 454-459
823 **Hetherington AJ, Bridson SL, Lee Jones A, Hass H, Kerp H, Dolan L** (2021) An
824 evidence-based 3D reconstruction of *Asteroxylon mackiei*, the most complex
825 plant preserved from the Rhynie chert. eLife **10:** e69447
826 **Hetherington AJ, Dolan L** (2017) The evolution of lycopsid rooting structures:
827 conservatism and disparity. New Phytol **215:** 538-544
828 **Hetherington AJ, Dolan L** (2018) Stepwise and independent origins of roots among
829 land plants. Nature **561:** 235-238
830 **Himanen K, Boucheron E, Vanneste S, de Almeida Engler J, Inzé D, Beeckman T**
831 (2002) Auxin-mediated cell cycle activation during early lateral root initiation.
832 Plant Cell **14:** 2339-2351
833 **Himanen K, Vuylsteke M, Vanneste S, Vercruysse S, Boucheron E, Alard P,**
834 **Chriqui D, Van Montagu M, Inzé D, Beeckman T** (2004) Transcript profiling
835 of early lateral root initiation. Proceedings of the National Academy of Sciences,
836 USA **101:** 5146-5151
837 **Hou G, Hill JP** (2004) Developmental anatomy of the fifth shoot-borne root in young
838 sporophytes of *Ceratopteris richardii*. Planta **219:** 212-220
839 **Huang L, Schiefelbein J** (2015) Conserved gene expression programs in developing
840 roots from diverse plants. Plant Cell **27:** 2119-2132
841 **Imaichi R, Kato M** (1989) Developmental anatomy of the shoot apical cell, rhizophore
842 and root of *Selaginella Uncinata*. Bot Mag Tokyo **102:** 369-380
843 **Jansen L, Hollunder J, Roberts I, Forestan C, Fonteyne P, Van Quickenborne C,**
844 **Zhen R-G, McKersie B, Parizot B, Beeckman T** (2013) Comparative
845 transcriptomics as a tool for the identification of root branching genes in maize.
846 Plant Biotechnol J **11:** 1092-1102
847 **Jones CS, Drinnan AN** (2009) The developmental pattern of shoot apices in
848 *Selaginella kraussiana* (Kunze) A. Braun. Int J Plant Sci **170:** 1009-1018

849 **Krtková J, Benáková M, Schwarzerová K** (2016) Multifunctional microtubule-
850 associated proteins in plants. Front Plant Sci **7:** 474
851 **Krtková J, Zimmermann A, Schwarzerová K, Nick P** (2012) Hsp90 binds
852 microtubules and is involved in the reorganization of the microtubular network
853 in angiosperms. J Plant Physiol **169:** 1329-1339
854 **Kurihara D, Mizuta Y, Sato Y, Higashiyama T** (2015) ClearSee: a rapid optical
855 clearing reagent for whole-plant fluorescence imaging. Development **142:**
856 4168-4179
857 **Langfelder P, Horvath S** (2008) WGCNA: an R package for weighted correlation
858 network analysis. BMC Bioinformatics **9:** 559
859 **Laskowski M, ten Tusscher KH** (2017) Periodic lateral root priming: what makes it
860 tick? Plant Cell **29:** 432-444
861 **Love MI, Huber W, Anders S** (2014) Moderated estimation of fold change and
862 dispersion for RNA-seq data with DESeq2. Genome Biol **15:** 550
863 **Lu K-J, van 't Wout Hofland N, Mor E, Mutte S, Abrahams P, Kato H, Vandepoele**
864 **K, Weijers D, De Rybel B** (2020) Evolution of vascular plants through
865 redeployment of ancient developmental regulators. Proc Natl Acad Sci USA **117:**
866 733-740
867 **Lu P, Jernstedt JA** (1996) Rhizophore and root development in *Selaginella martensii*:
868 meristem transitions and identity. Int J Plant Sci **157:** 180-194
869 **Magyar Z, Horváth B, Khan S, Mohammed B, Henriques R, De Veylder L, Bakó**
870 **L, Scheres B, Bögre L** (2012) *Arabidopsis* E2FA stimulates proliferation and
871 endocycle separately through RBR-bound and RBR-free complexes. EMBO J
872 **31:** 1480-1493
873 **Marhavý P, Vanstraelen M, De Rybel B, Ding Z, Bennett MJ, Beeckman T,**
874 **Benková E** (2013) Auxin reflux between the endodermis and pericycle
875 promotes lateral root initiation. EMBO J **32:** 149-158
876 **Matsunaga KKS, Tomescu AMF** (2016) Root evolution at the base of the lycophyte

877 clade: insights from an Early Devonian lycophyte. Ann Bot **117:** 585-598
878 **Moreno-Risueno MA, Van Norman JM, Moreno A, Zhang J, Ahnert SE, Benfey**
879 **PN** (2010) Oscillating gene expression determines competence for periodic
880 *Arabidopsis* root branching. Science **329:** 1306-1311
881 **Motte H, Beeckman T** (2019) The evolution of root branching: increasing the level of
882 plasticity. J Exp Bot **70:** 785-793
883 **Motte H, Parizot B, Fang T, Beeckman T** (2020) The evolutionary trajectory of root
884 stem cells. Curr Opin Plant Biol **53:** 23-30
885 **Motte H, Vanneste S, Beeckman T** (2019) Molecular and environmental regulation of
886 root development. Annu Rev Plant Biol **70:** 465-488
887 **Müller B, Sheen J** (2008) Cytokinin and auxin interaction in root stem-cell
888 specification during early embryogenesis. Nature **453:** 1094-1097
889 **Okushima Y, Overvoorde PJ, Arima K, Alonso JM, Chan A, Chang C, Ecker JR,**
890 **Hughes B, Lui A, Nguyen D, et al** (2005) Functional genomic analysis of the
891 *AUXIN RESPONSE FACTOR* gene family members in *Arabidopsis thaliana*:
892 unique and overlapping functions of *ARF7* and *ARF19*. Plant Cell **17:** 444-463
893 **Oltmanns F** (1889) Beiträge zur Kenntniss der Fucaceen. Bibliotheca Botanica **14:** 1-
894 94
895 **Otręba P, Gola EM** (2011) Specific intercalary growth of rhizophores and roots in
896 *Selaginella kraussiana* (Selaginellaceae) is related to unique dichotomous
897 branching. Flora **206:** 227-232
898 **Patro R, Duggal G, Love MI, Irizarry RA, Kingsford C** (2017) Salmon provides fast
899 and bias-aware quantification of transcript expression. Nat Methods **14:** 417-
900 419
901 **Ramakrishna P, Ruiz Duarte P, Rance GA, Schubert M, Vordermaier V, Vu LD,**
902 **Murphy E, Vilches Barro A, Swarup K, Moirangthem K, et al** (2019)
903 EXPANSIN A1-mediated radial swelling of pericycle cells positions anticlinal
904 cell divisions during lateral root initiation. Proc Natl Acad Sci USA **116:** 8597-

905 8602
906 **Raven JA, Edwards D** (2001) Roots: evolutionary origins and biogeochemical
907 significance. J Exp Bot **52:** 381-401
908 **Ritchie ME, Phipson B, Wu D, Hu Y, Law CW, Shi W, Smyth GK** (2015) *limma*
909 powers differential expression analyses for RNA-sequencing and microarray
910 studies. Nucleic Acids Res **43:** e47
911 **Ryu KH, Huang L, Kang HM, Schiefelbein J** (2019) Single-cell RNA sequencing
912 resolves molecular relationships among individual plant cells. Plant Physiol **179:**
913 1444-1456
914 **Shimotohno A, Heidstra R, Blilou I, Scheres B** (2018) Root stem cell niche organizer
915 specification by molecular convergence of PLETHORA and SCARECROW
916 transcription factor modules. Genes Dev **32:** 1085-1100
917 **Shulse CN, Cole BJ, Ciobanu D, Lin J, Yoshinaga Y, Gouran M, Turco GM, Zhu**
918 **Y, O'Malley RC, Brady SM, et al** (2019) High-throughput single-cell
919 transcriptome profiling of plant cell types. Cell Reports **27:** 2241-2247
920 **Stahl Y, Wink RH, Ingram GC, Simon R** (2009) A signaling module controlling the
921 stem cell niche in *Arabidopsis* root meristems. Curr Biol **19:** 909-914
922 **Tian F, Yang D-C, Meng Y-Q, Jin J, Gao G** (2019) PlantRegMap: charting functional
923 regulatory maps in plants. Nucleic Acids Res **48:** D1104-D1113
924 **Truernit E, Bauby H, Dubreucq B, Grandjean O, Runions J, Barthélémy J,**
925 **Palauqui J-C** (2008) High-resolution whole-mount imaging of three-
926 dimensional tissue organization and gene expression enables the study of
927 phloem development and structure in *Arabidopsis*. Plant Cell **20:** 1494-1503
928 **Van Bel M, Diels T, Vancaester E, Kreft L, Botzki A, Van de Peer Y, Coppens F,**
929 **Vandepoele K** (2018) PLAZA 4.0: an integrative resource for functional,
930 evolutionary and comparative plant genomics. Nucleic Acids Res **46:** D1190-
931 D1196
932 **van den Hoek C, Mann DG, Jahns HM** (1995) Algae: an introduction to phycology.

933 Cambridge University Press, Groningen, Edingurgh and Düsseldorf
934 **Van Norman JM, Zhang J, Cazzonelli CI, Pogson BJ, Harrison PJ, Bugg TDH,**
935 **Chan KX, Thompson AJ, Benfey PN** (2014) Periodic root branching in
936 *Arabidopsis* requires synthesis of an uncharacterized carotenoid derivative.
937 Proc Natl Acad Sci USA **111:** E1300-E1309
938 **Vandepoele K, Van Bel M, Richard G, Van Landeghem S, Verhelst B, Moreau H,**
939 **Van de Peer Y, Grimsley N, Piganeau G** (2013) pico-PLAZA, a genome
940 database of microbial photosynthetic eukaryotes. Environ Microbiol **15:** 2147-
941 2153
942 **Vanneste S, De Rybel B, Beemster GTS, Ljung K, De Smet I, Van Isterdael G,**
943 **Naudts M, Iida R, Gruissem W, Tasaka M, et al** (2005) Cell cycle progression
944 in the pericycle is not sufficient for SOLITARY ROOT/IAA14-mediated lateral
945 root initiation in *Arabidopsis thaliana*. Plant Cell **17:** 3035-3050
946 **Vermeer JEM, Geldner N** (2015) Lateral root initiation in *Arabidopsis thaliana*: a
947 force awakens. F1000Prime Rep **7:** 32
948 **Vermeer JEM, von Wangenheim D, Barberon M, Lee Y, Stelzer EHK, Maizel A,**
949 **Geldner N** (2014) A spatial accommodation by neighboring cells is required for
950 organ initiation in *Arabidopsis*. Science **343:** 178-183
951 **von Goebel K** (1928) Organographie der pflanzen: allgemeine organographie, Ed 3.
952 Fischer, Jena, Germany
953 **Wildwater M, Campilho A, Perez-Perez JM, Heidstra R, Blilou I, Korthout H,**
954 **Chatterjee J, Mariconti L, Gruissem W, Scheres B** (2005) The
955 *RETINOBLASTOMA-RELATED* gene regulates stem cell maintenance in
956 *Arabidopsis* roots. Cell **123:** 1337-1349
957 **Wu C-C, Li F-W, Kramer EM** (2019) Large-scale phylogenomic analysis suggests
958 three ancient superclades of the WUSCHEL-RELATED HOMEOBOX
959 transcription factor family in plants. PLoS ONE **14:** e0223521
960 **Xuan W, Audenaert D, Parizot B, Möller BK, Njo M F, De Rybel B, De Rop G,**

961 **Van Isterdael G, Mähönen A P, Vanneste S, et al** (2015) Root cap-derived
962 auxin pre-patterns the longitudinal axis of the *Arabidopsis* root. Curr Biol **25:**
963 1381-1388
964 **Xuan W, Band LR, Kumpf RP, Van Damme D, Parizot B, De Rop G, Opdenacker**
965 **D, Möller BK, Skorzinski N, Njo MF, et al** (2016) Cyclic programmed cell
966 death stimulates hormone signaling and root development in *Arabidopsis*.
967 Science **351:** 384-387
968 **Zhang T-Q, Xu Z-G, Shang G-D, Wang J-W** (2019) A single-cell RNA sequencing
969 profiles the developmental landscape of *Arabidopsis* root. Mol Plant **12:** 648-
970 660
971 **Zhou X, Guo Y, Zhao P, Sun M-x** (2018) Comparative analysis of WUSCHEL-related
972 homeobox genes revealed their parent-of-origin and cell type-specific
973 expression pattern during early embryogenesis in tobacco. Front Plant Sci **9:**
974 311
975 **Zhu C, Dixit R** (2012) Functions of the *Arabidopsis* kinesin superfamily of
976 microtubule-based motor proteins. Protoplasma **249:** 887-899
977

978

979

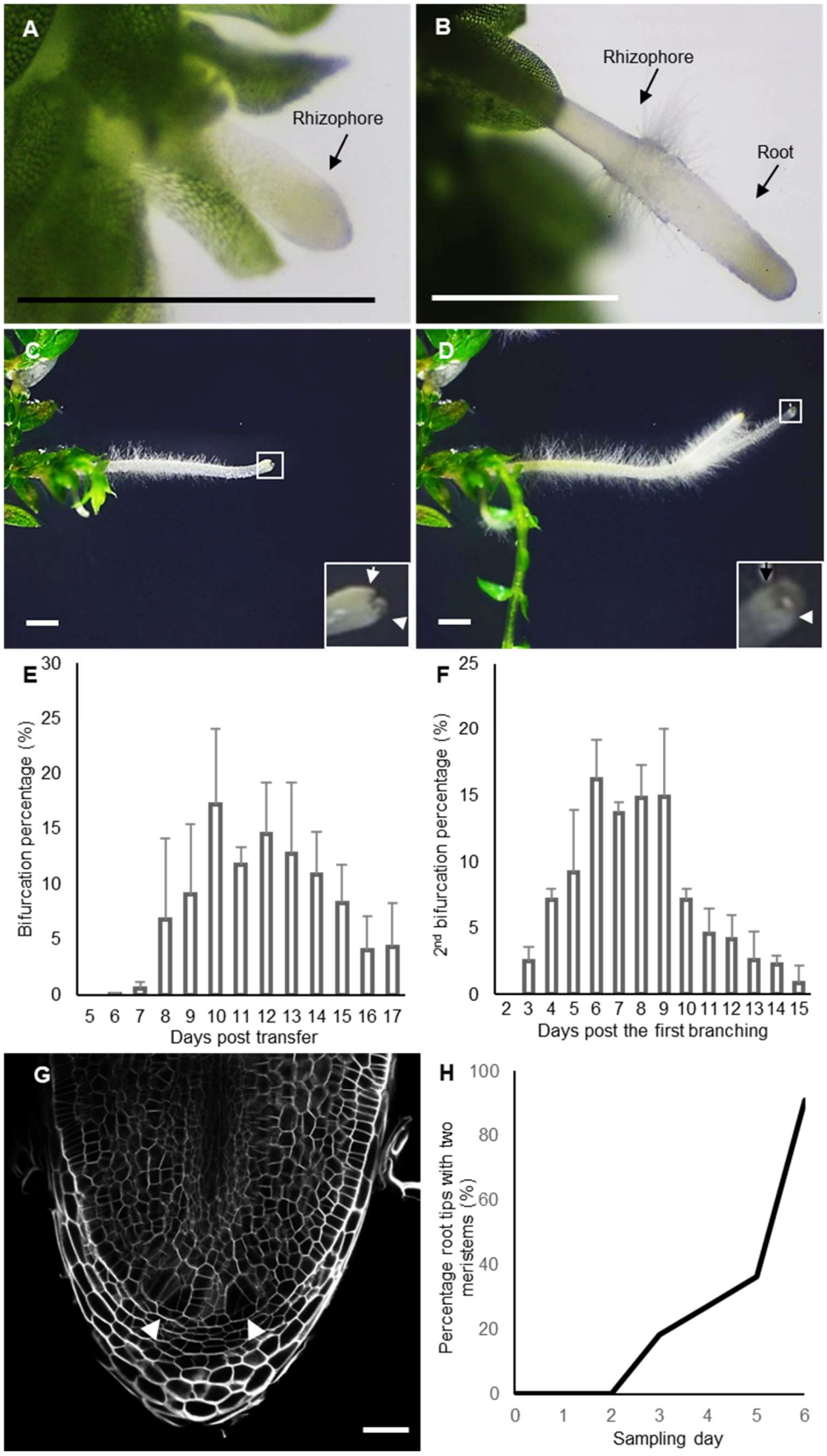
A
Rhizophore
B
Rhizophore
Root
C
D
E
Bifurcation percentage (%)
Days post transfer
F
2nd bifurcation percentage (%)
Days post the first branching
G
H
Percentage root tips with two meristems (%)
Sampling day

980

Figure 1. Dichotomous root branching in *Selaginella moellendorffii*. A, A young hairless rhizophore. B, Root emergence from the rhizophore. The transition from the rhizophore to the root is marked by the appearance of a collar of root hairs. Scale bars: 0.1 mm. C and D, Formation of first (C) and second (D) order bifurcated roots. The insets are magnifications of the squares. The arrows indicate newly formed root apices. Scale bars: 1 mm. E, Percentage of root tips that underwent the first bifurcation during 17 d after transfer on 1/2 MS. The bifurcation percentage was calculated as the number of bifurcated roots divided by the total number of roots. Values are averages of 3 repeats ± SD. F, Percentage of root tips that underwent the second bifurcation during 15 d after the first bifurcation. . The bifurcation percentage was calculated as the number of secondly bifurcated root apices divided by the total number of the apices from roots that underwent a first bifurcation. Values are averages of 2 repeats ± SD. G, Confocal image showing a bifurcated apical meristem: root tip with two new clearly recognizable young meristems (arrowheads). Scale bar: 50 μm. H, Percentage of bifurcated meristems in the root branching time course setup, i.e. days after the first branching. The percentage in Figure 1H was calculated as the number of root apices showing clear apical meristem bifurcation (see Fig. 1G) divided by the total number of sampled root tips. n (daily sample number) ≥ 10.

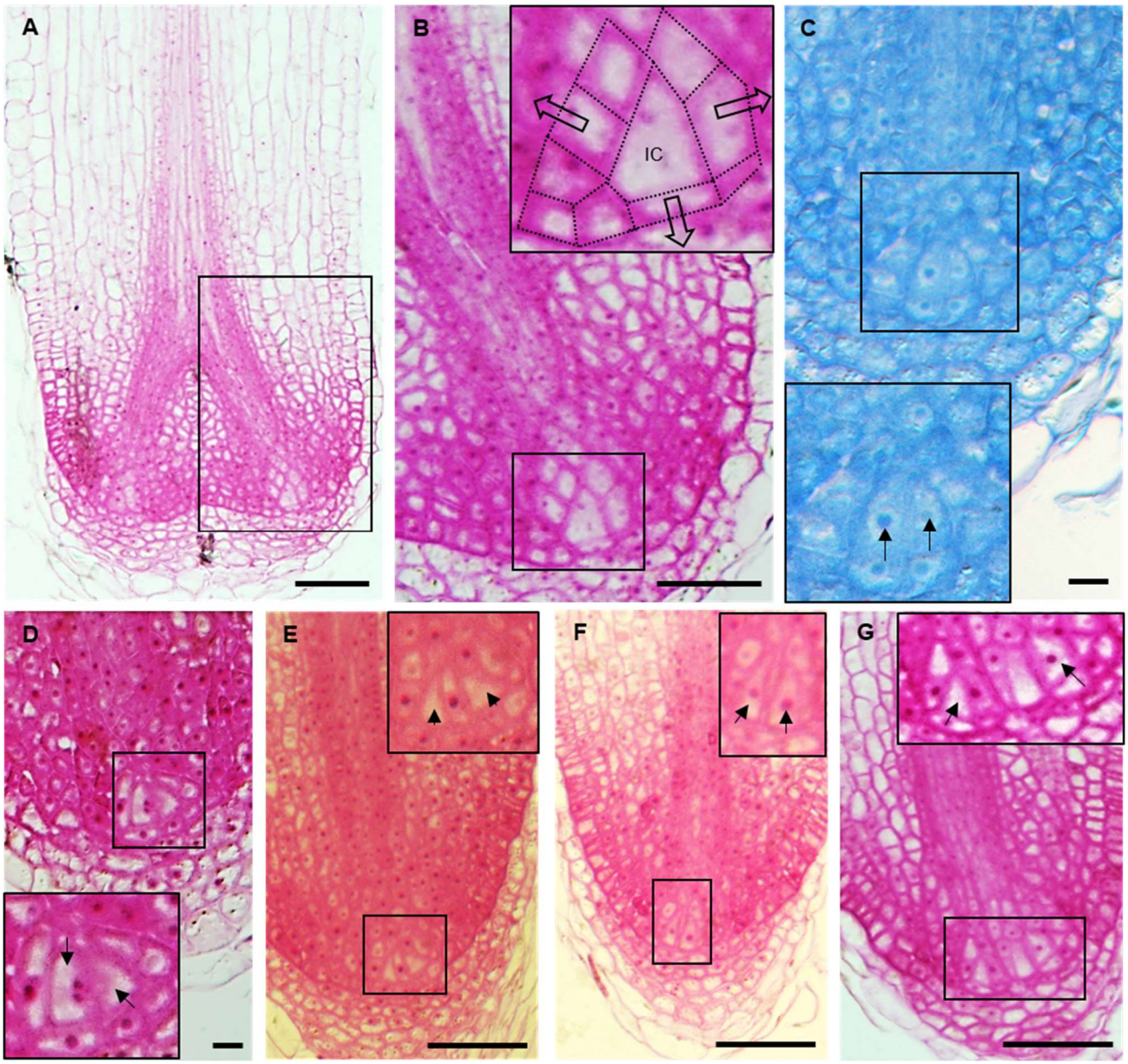

Figure 2. Histological sections from *S. moellendorffii* roots sampled during the root branching time course. A and B, A newly branched root tip containing two apical meristems sampled on day 0, (B) is a magnification of the indicated area in (A). The inset in (B) shows a magnification of the initial cell (IC) and its neighboring region. The initial and the presumptive most recent daughter cells are indicated by dotted lines. The hollow arrows indicate the expected directions in which the IC cuts off daughter cells from the different faces. C-G, Early-stage bifurcating meristems with two presumptive ICs next or close to each other. The insets shows a magnification of the indicated area, the arrows indicate the ICs. Scale bars: 50 µm, except for panel (C) and (D): 10 µm.

1015

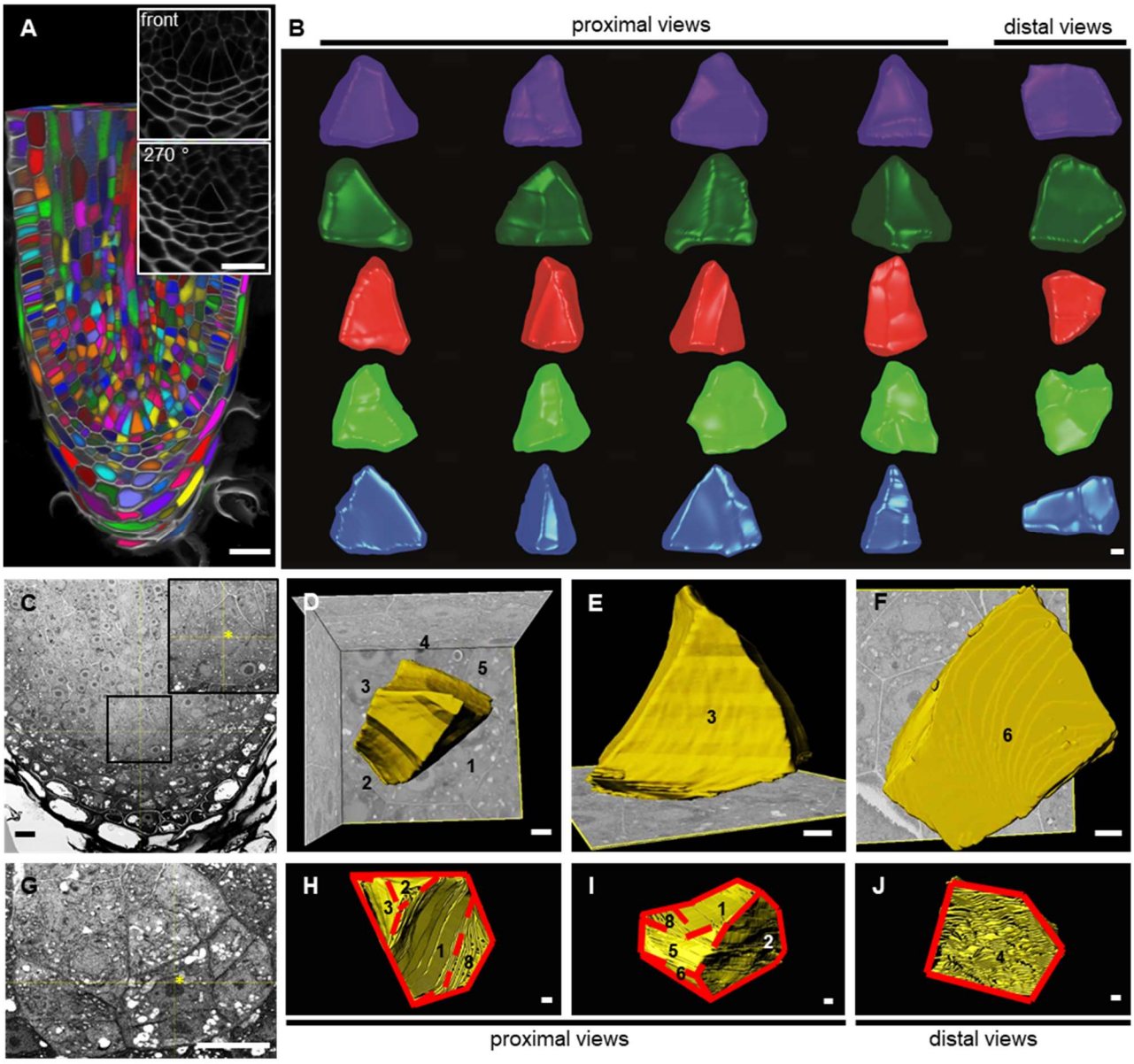

Figure 3. 3D imaging to segment ICs. A, Example of a *S. moellendorffii* root generated from a whole-mount confocal stack (Supplemental Movie S2). Individual cells are randomly colored. Insets show magnifications of the front view or the 270 degree turned view. Scale bars: 20 µm. B, Different views of five ICs segmented from confocal stacks. The fifth IC was segmented from the root in panel A. See Supplemental Movies S3-S7 for a full overview of the ICs Scale bar: 2 µm. C and G, SBF-SEM longitudinal sections (xz-views) showing two ICs. The inset shows a magnification of the indicated area in (C). The asterisks indicate the ICs. Scale bars: 10 µm. D-F and H-J, Serial section reconstruction of the ICs. The numbers indicate the corresponding faces of the cells. See Supplemental Movies S8 and S9 for a full overview. The solid and dashed lines in (H-J) separate the different faces. Scale bars: 1 µm.

1030

1031

1032

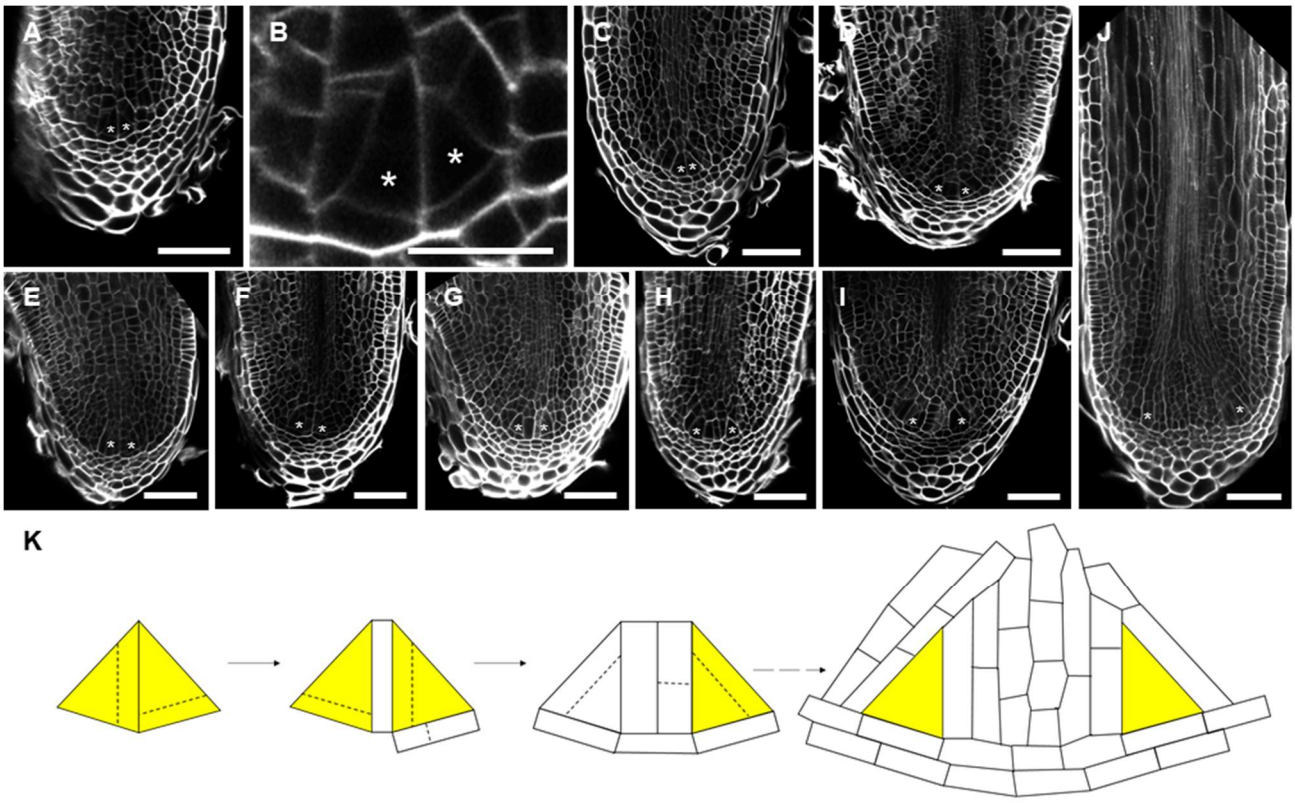
A
B
C
D
J
E
F
G
H
I
K

1034 **Figure 4.** Early stages during *S. moellendorffii* root bifurcation. A-J, Confocal images
1035 of different stages during branching sampled between 1 and 5 days in the root branching
1036 time course. (B) shows a magnification of the root in (A). Scale bars are 50 µm, except
1037 for (B), where it is 20 µm. Asterisks indicate the location of the ICs. A-C, Two ICs are
1038 next to each other. See Supplemental Figure S2, A-C for more examples. E-G, Two ICs
1039 are only separated by one or two layers of cells. See Supplemental Figure S2, D-F for
1040 more examples. H-I, Further development of the two meristems, including enlargement
1041 of the root tip. K, Scheme showing the mechanism of root bifurcation as deduced from
1042 independent root samples during the early time points of root branching. Dashed lines
1043 indicate possible cell divisions.
1044

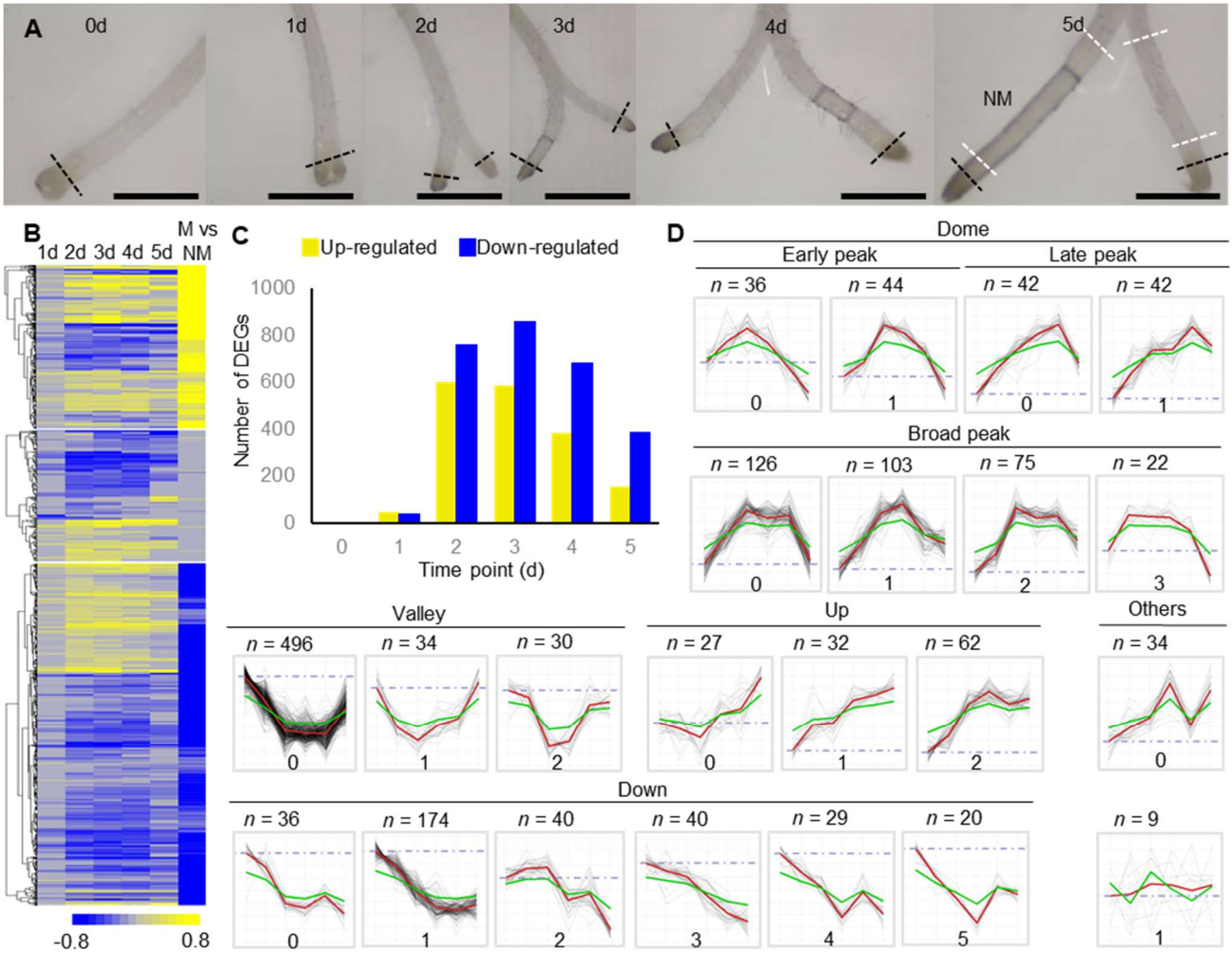

Figure 5. *S. moellendorffii* root branching transcriptome. A, Experimental set-up, showing sampled regions (dotted black lines: meristematic region; white: non-meristematic region (NM)). Scale bars are 1 mm. B, Heatmap showing expression [$\log_2$ fold change (FC)] of all root branching genes on the different days in the root branching course versus day 0, or for the meristematic (M) versus non-meristematic (NM) region. Gray values indicate no significance. C, Overview of numbers of up-regulated and downregulated differentially expressed genes (DEGs) at each time point during root branching. Note the decrease in number at the end of the time course, indicating a return to the initial state. D, Profiles of co-expression clusters based on weighted gene co-expression network analysis (WGCNA) of the root branching genes. Clusters were grouped according to their shapes: Dome and Valley groups – the transiently upregulated and downregulated clusters, respectively; Up and Down groups – constitutively upregulated and downregulated clusters, respectively. Based on the peak position and shape, the Dome group was further grouped into Early peak, Late peak and Broad peak subgroups. In each cluster, the red curve represents the average expression of all genes in the cluster, and the green curve represents the eigengene of the cluster.

1064

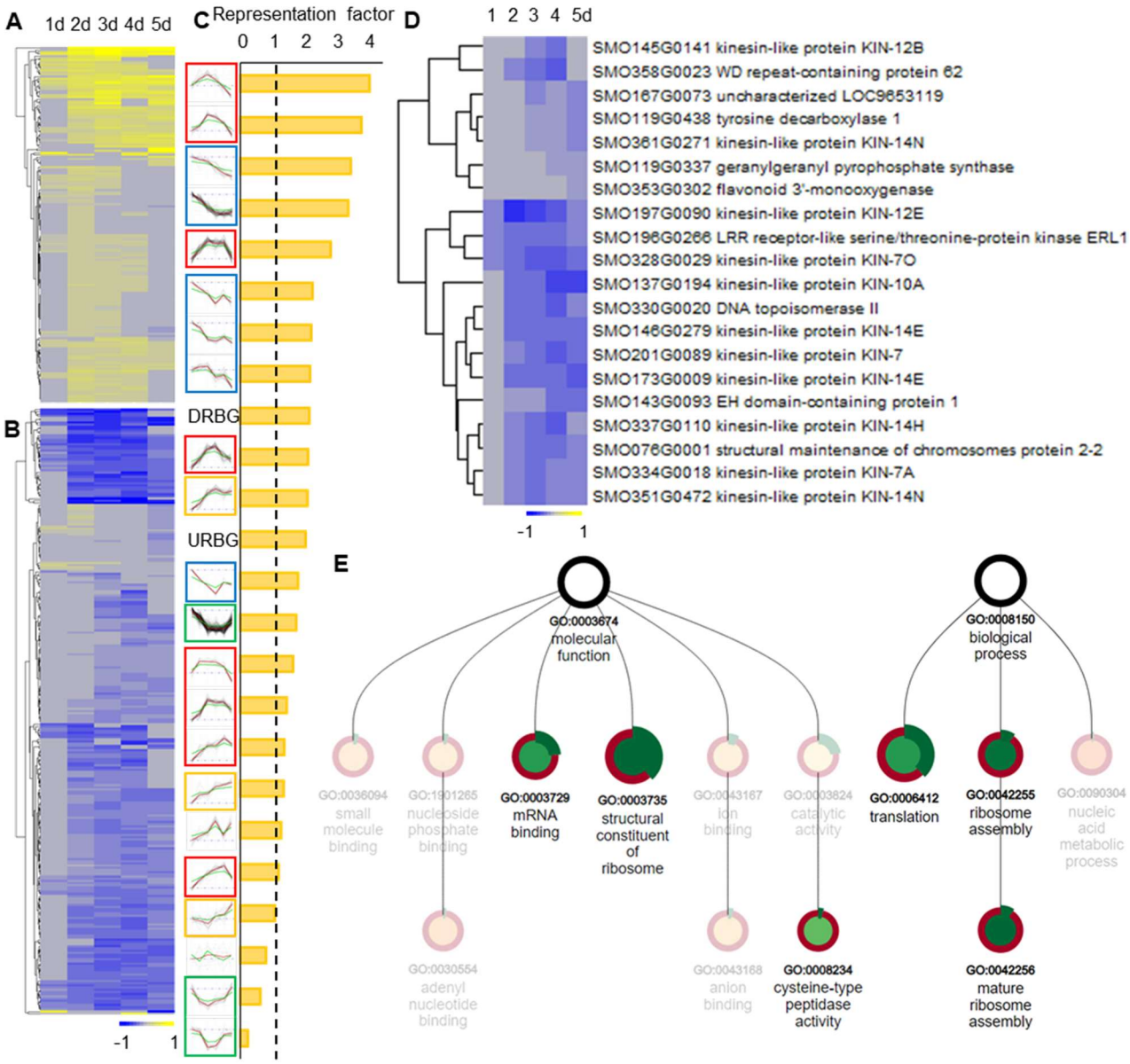

Figure 6. Overview of root branching meristem-enriched genes. A and B, The heatmaps show the expression [$\log_2$ fold change (FC)] of meristem-enriched genes upregulated (A) or downregulated (B) during root branching. C, Representation of the meristem-enriched genes in different expression clusters. The meristem-enriched genes were in particular overrepresented in transiently upregulated (Dome) clusters in red frames and constitutively downregulated (Down) clusters in blue frames. Orange and green frames indicate constitutively upregulated (Up) and transiently downregulated (Valley) clusters, respectively. DRBG, Downregulated root branching genes; URBG, Upregulated root branching genes. D, Heat map showing the expression [$\log_2$ fold change (FC)] the top 20 meristem-enriched genes that were downregulated during root branching. The descriptions of the genes were retrieved from Phytozome (JGI) or NCBI. E, Enrichment

1079 analysis of the meristem-enriched genes that were upregulated during root branching.
1080 The graph shows enriched Molecular Function and Biological Process Gene Ontology
1081 (GO) terms. Node size is scaled by the *p*-value of the enriched GO term, and node color
1082 (from green to red) is determined by the enrichment fold of the term. Negative
1083 enrichment folds are faded. The outer green band is determined by the subset ratio. The
1084 graph was generated by PLAZA version 4.5
1085 (https://bioinformatics.psb.ugent.be/plaza/versions/plaza_v4_5_dicots/).

1086

1087

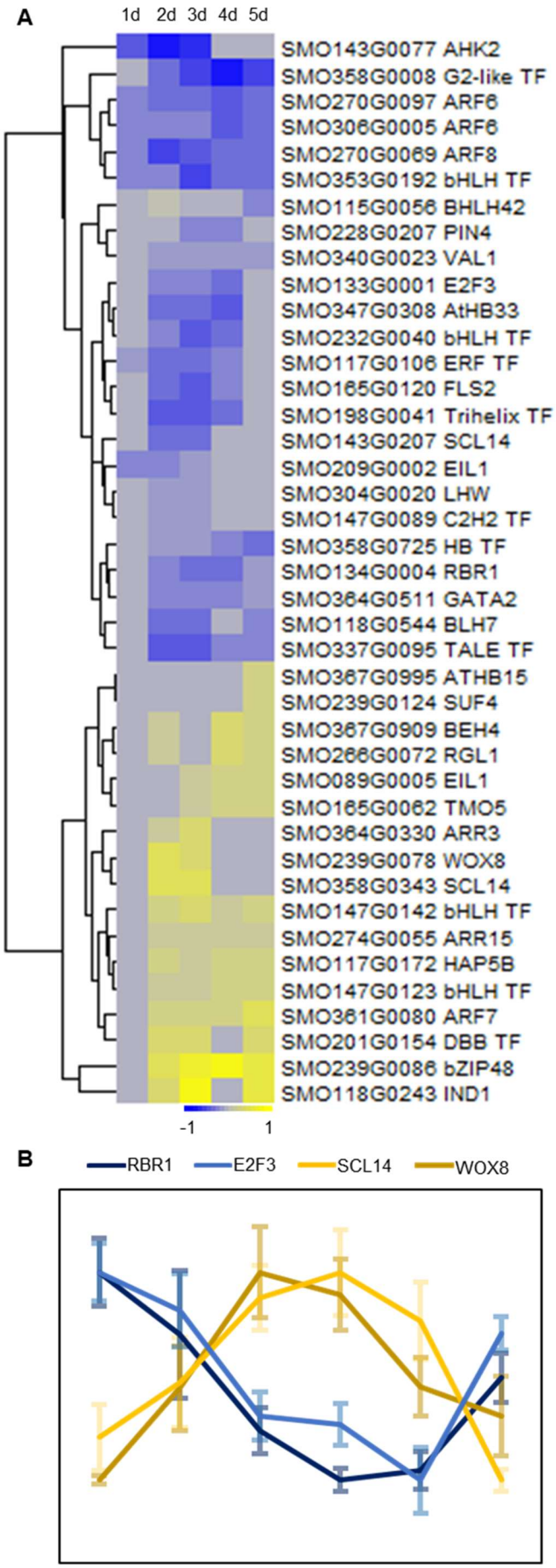
A
1d 2d 3d 4d 5d
SMO143G0077 AHK2
SMO358G0008 G2-like TF
SMO270G0097 ARF6
SMO306G0005 ARF6
SMO270G0069 ARF8
SMO353G0192 bHLH TF
SMO115G0056 BHLH42
SMO228G0207 PIN4
SMO340G0023 VAL1
SMO133G0001 E2F3
SMO347G0308 AtHB33
SMO232G0040 bHLH TF
SMO117G0106 ERF TF
SMO165G0120 FLS2
SMO198G0041 Trihelix TF
SMO143G0207 SCL14
SMO209G0002 EIL1
SMO304G0020 LHW
SMO147G0089 C2H2 TF
SMO358G0725 HB TF
SMO134G0004 RBR1
SMO364G0511 GATA2
SMO118G0544 BLH7
SMO337G0095 TALE TF
SMO367G0995 ATHB15
SMO239G0124 SUF4
SMO367G0909 BEH4
SMO266G0072 RGL1
SMO089G0005 EIL1
SMO165G0062 TMO5
SMO364G0330 ARR3
SMO239G0078 WOX8
SMO358G0343 SCL14
SMO147G0142 bHLH TF
SMO274G0055 ARR15
SMO117G0172 HAP5B
SMO147G0123 bHLH TF
SMO361G0080 ARF7
SMO201G0154 DBB TF
SMO239G0086 bZIP48
SMO118G0243 IND1
-1
1
B
RBR1
E2F3
SCL14
WOX8

1088

1089 **Figure 7.** Expression profiles of the transcription factors encoding DEGs and other
1090 genes with their Arabidopsis homologs known to be involved in root meristem control
1091 or lateral root (LR) formation. A, Heatmap showing the expression [$\log_2$ fold change
1092 (FC)] profiles. The description shows the best Arabidopsis hit according to Banks et al.
1093 (2011) or, if not present, the transcription factor type was retrieved according to Plant
1094 Transcription Factor Database (PlantTFDB) v5. B, Relative expression of homologs of
1095 *RETINOBLASTOMA-RELATED1* (*RBR1*), *E2F TRANSCRIPTION FACTOR-3* (*E2F3*),
1096 *SCARECROW* (*SCR*) (*SCR-LIKE14* (*SCL14*)), and the *WUSCHEL RELATED*
1097 *HOMEOBOX* (*WOX*) family (*WOX8*). Error bars indicate SE (n = 4).
1098

Supplemental data

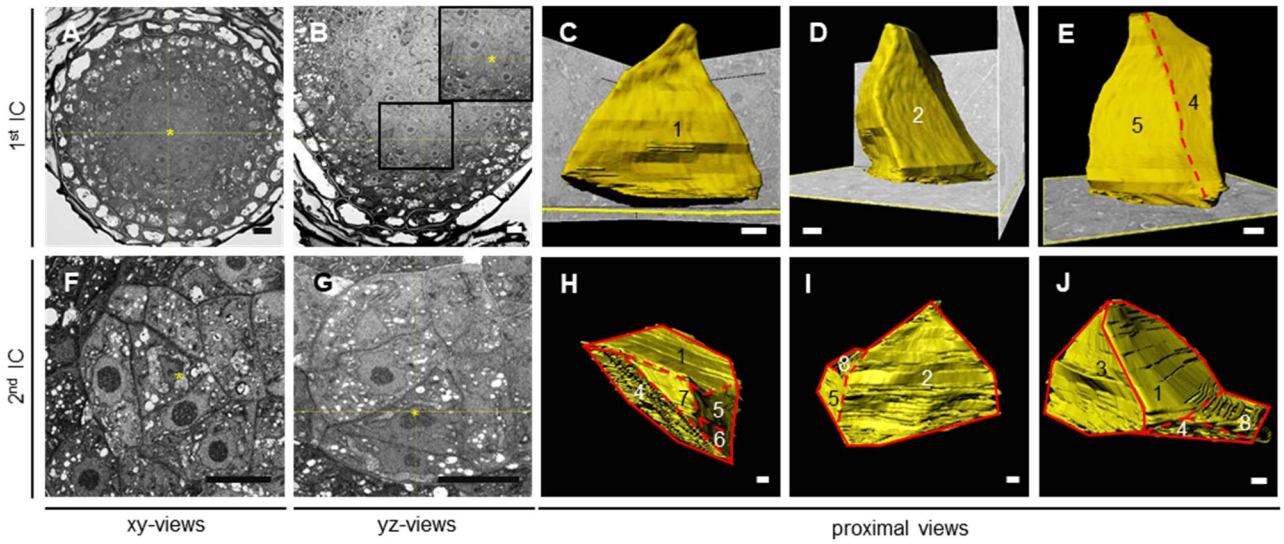

Supplemental Figure S1. Additional SBF-SEM images and proximal views of the reconstructed root ICs in *S. moellendorffii*. (A-E) show the first IC and (F-J) show the second. (A and F) and (B and G) are transverse (xy) and longitudinal (yz) SBF-SEM sections, respectively. The inset shows a magnification of the indicated area in (B). The asterisks indicate the ICs. Scale bars: 10 µm. (C-E) and (H-J) show other proximal views of the reconstructed ICs, demonstrating that the ICs are not tetrahedral. The numbers indicate the corresponding faces of the cells. The solid and dashed lines in (H-J) indicate the main lines and the ones relatively difficult to be recognized, repectively. Scale bars: 1 µm.

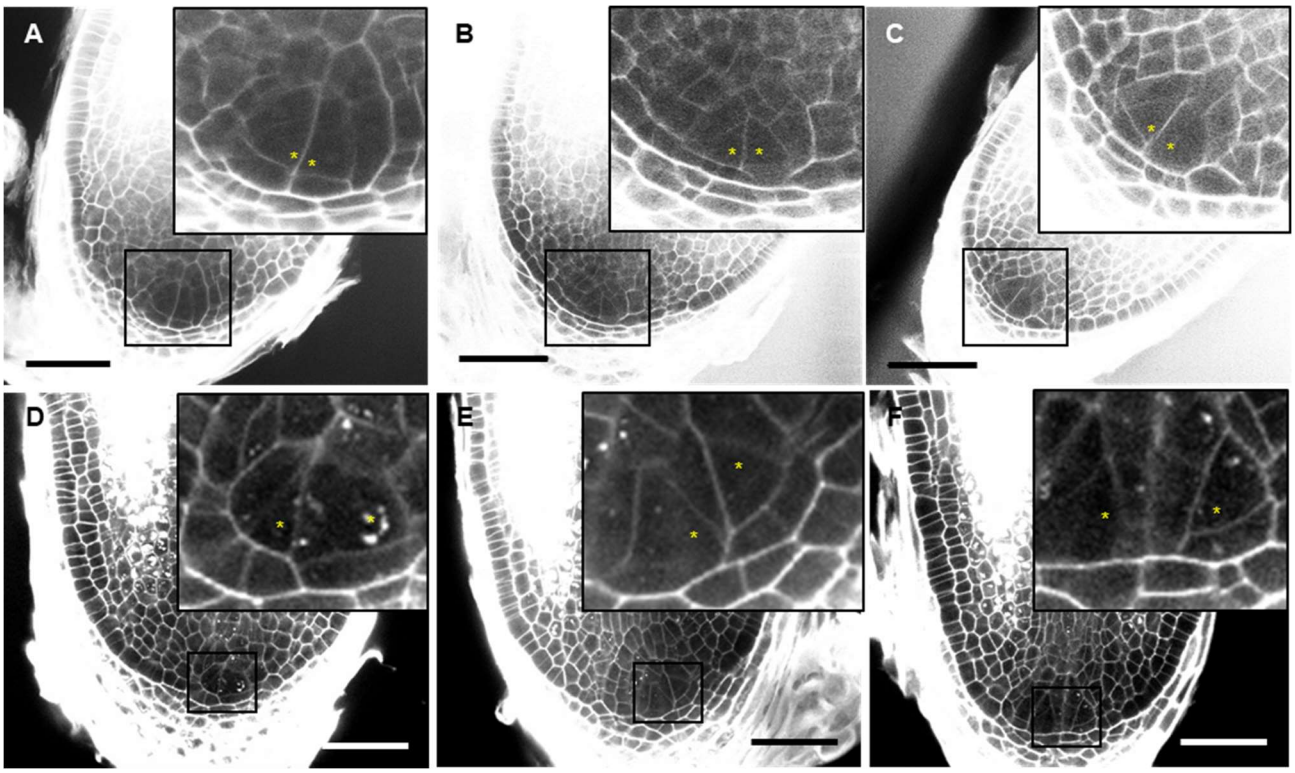

Supplemental Figure S2. Additional confocal images taken during the root branching assay in *S. moellendorffii*. A-C, More examples of symmetric division of the original IC resulting in two new initials. D-F, More examples showing two initials that are only separated by one or two layers of cells, further supporting that they originated next to each other. Scale bars: 50 µm.